Hybrid Post-Tensioned Precast Concrete Walls for Use in Seismic Regions

Yahya C. Kurama, Ph.D., P.E.
Assistant Professor
Civil Engineering and
Geological Sciences
University of Notre Dame
Notre Dame, Indiana

Recent research has shown that post-tensioned precast concrete lateral load resisting walls that do not emulate the behavior of monolithic cast-in-place reinforced concrete walls have desirable seismic characteristics such as a self-centering capability and an ability to undergo nonlinear lateral displacements with little damage. The biggest disadvantage of these walls under earthquake loading is an increase in the lateral displacements as a result of small energy dissipation. This paper investigates a "hybrid" precast wall system that uses mild steel reinforcement in addition to the post-tensioning steel for flexural strength and inelastic energy dissipation. An analytical parametric study is conducted to compare the expected seismic behavior of a series of prototype walls with different amounts of mild steel and post-tensioning steel. Nonlinear dynamic time history analyses of the walls indicate that the use of mild steel reinforcement results in a considerable reduction in the lateral displacements of the walls under earthquake loading, particularly for walls in regions of high seismicity and with shorter periods of vibration. The results of these analyses are used to present preliminary design implications for the use of hybrid post-tensioned precast walls in seismic regions.

In recent years, a significant amount of research has been conducted on precast concrete wall systems for seismic regions of the United States as a part of the PRESSS (PREcast Seismic Structural Systems) research program[1-3] and other research programs.[4-6] One of the precast wall systems that has successfully emerged from the PRESSS program is the unbonded post-tensioned wall system.

As an example, Fig. 1(a) shows the elevation and cross section of a six-story wall, which is constructed by post-tensioning precast wall panels across horizontal joints using high strength post-tensioning bars that are not bonded to the concrete.[1,2] The post-tensioning (PT) bars are placed inside oversize ducts that are not grouted, and they are anchored only at the roof and at the foundation. The

bars provide flexural reinforcement to the wall to resist lateral loads.

Dry-pack or grout may be used between the wall panels to maintain construction tolerances and alignment. Spiral reinforcing steel is used in the base panel to confine the concrete near the ends of the wall at the base. Wire mesh is used as bonded steel reinforcement in the wall panels. The wire mesh reinforcement is not continuous across the horizontal joints and, thus, does not contribute to the flexural strength of the wall.

Under lateral loads, the desired nonlinear behavior of unbonded post-tensioned precast walls is an axial-flexural behavior that is governed by the opening of discrete gaps along the horizontal joints between the wall panels and between the wall and the foundation [see Fig. 1(a)].[1,2] A design approach to achieve this behavior in the walls under earthquake loading is explained in Kurama et al.[1]

The opening of the first gap in a wall is expected to occur along the base-panel-to-foundation joint when the precompression stresses at the base of the wall due to gravity and post-tensioning loads are overcome by the flexural stresses that develop at the tension side of the wall due to the lateral loads.[1,2]

The opening of the gaps along the horizontal joints occurs with little or no cracking in the wall panels since the post-tensioning bars are not bonded to the concrete and, thus, the stress transfer between the post-tensioning steel and the concrete due to bond is eliminated. The size of the gaps is controlled by the restoring effect of the post-tensioning steel, which develops as the bars are stretched (i.e., elongated) due to the opening of the gaps. This restoring force closes the gaps upon unloading of the wall from a nonlinear lateral displacement.

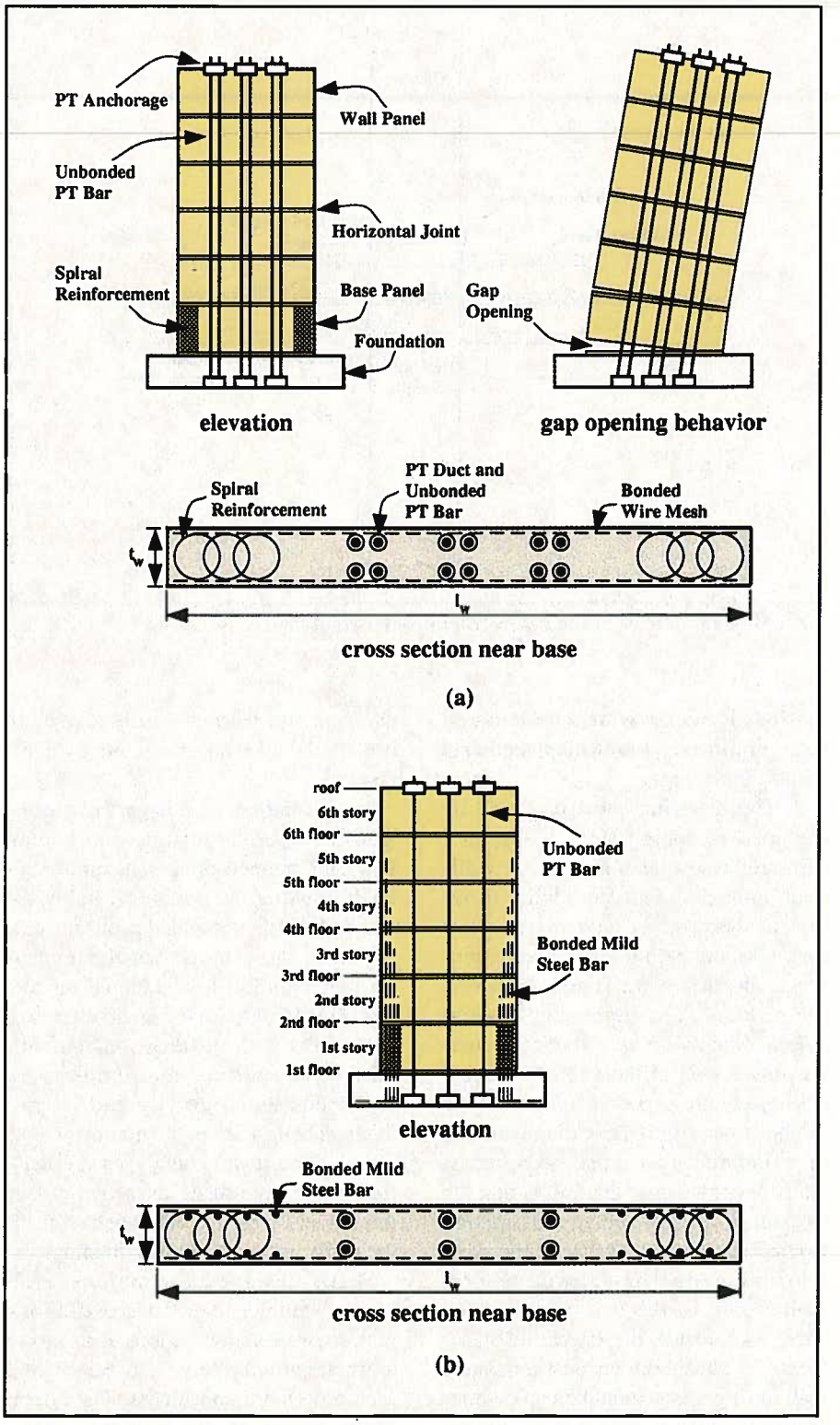

Fig. 1. Precast walls: (a) unbonded post-tensioned wall; (b) hybrid wall.

As a result of the use of unbonded steel bars as flexural reinforcement and the opening of discrete gaps along the horizontal joints, the behavior of unbonded post-tensioned precast walls under lateral loads is significantly different from the behavior of flexural monolithic cast-in-place reinforced concrete walls (i.e., cast-in-place walls with behavior under lateral loads governed by flexural deformations rather than shear deformations). Compared with monolithic cast-in-place walls, unbonded post-tensioned walls are expected to have the following desirable seismic characteristics:[1,2]

1. The use of unbonded bars results in a uniform strain distribution in the post-tensioning steel and, thus, the nonlinear straining (i.e., yielding) of the post-tensioning steel during the lateral displacements of a wall is significantly delayed or prevented. Furthermore, cracking in the wall panels is reduced. Compared with monolithic cast-in-place walls, unbonded post-

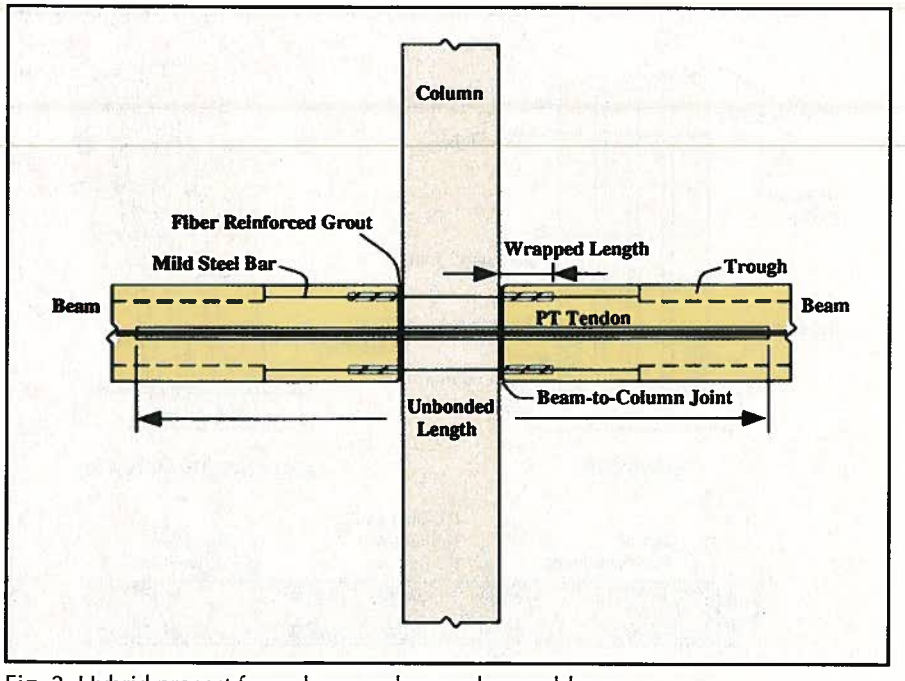

Fig. 2. Hybrid precast frame beam-column subassemblage.

tensioned precast walls can undergo large nonlinear lateral displacements with little damage.

2. The restoring force provided by the post-tensioning steel results in a self-centering capability of the walls upon unloading (i.e., an ability to return to the original undisplaced position upon unloading from a large nonlinear displacement). This means that the residual (i.e., permanent) lateral displacements of an unbonded post-tensioned wall at the end of a severe earthquake are expected to be small.

The most significant disadvantage of unbonded post-tensioned precast walls under seismic loading is that the amount of inelastic energy dissipation is small since the yielding of the post-tensioning steel is delayed or prevented due to the use of unbonded bars. As a result, the lateral displacements of an unbonded post-tensioned wall during an earthquake can be considerably larger than the displacements of a comparable monolithic cast-in-place reinforced concrete wall.[1,4,5]

In order to increase the amount of energy dissipation, the use of supplemental metallic-yield dampers along vertical joints between two or more walls has been investigated experimentally by Priestley et al.[3] and analytically by Perez.[6] The use of friction dampers and viscous fluid dampers in the walls was investigated by Kurama.[4,5]

As an alternative, this paper investigates a "hybrid" precast wall system that uses bonded mild steel reinforcement crossing the horizontal joints, in addition to the unbonded post-tensioning steel. First, an analytical parametric investigation is conducted on the nonlinear behavior of twelve prototype walls with different amounts of mild steel and post-tensioning steel under combined gravity and lateral loads. Then, a series of nonlinear dynamic time history analyses are carried out to investigate the effect of the mild steel on the expected behavior of the walls under earthquake loading.

Walls designed for regions with high seismicity (e.g., coastal California), as well as for regions with moderate seismicity (e.g., Boston, Massachusetts), are considered. The effect of the number of stories on the behavior of the walls is investigated. Based on the results from the parametric analyses, preliminary recommendations for the use of the walls as primary lateral load resisting systems in seismic regions are provided. These recommendations may be useful as background in the development of seismic design guidelines for hybrid precast walls.

HYBRID PRECAST SYSTEMS

As an alternative to using supplemental energy dissipation devices such as metallic-yield, friction, and viscous fluid dampers, it is also possible to reduce the seismic displacements of unbonded post-tensioned precast walls by using bonded deformed mild steel reinforcement crossing the horizontal joints, particularly the base-panel-to-foundation joint as shown in Fig. 1(b). Properly designed and detailed mild steel reinforcement will yield in tension and compression during the cyclic lateral displacements of a wall, thus dissipating energy.

The concept of combining post-tensioning steel for flexural strength and self-centering with mild steel for inelastic energy dissipation has been previously applied to beam-to-column joints in precast concrete lateral load resisting frames at the National Institute of Standards and Technology (NIST)[7-9] and at the University of California at San Diego.[3,10]

As an example, Fig. 2 shows a hybrid precast frame beam-column subassemblage with multi-strand post-tensioning tendons and mild steel bars used through the beam-to-column joints. The mild steel bars are located near the top and bottom of the beams in order to maximize the nonlinear strains in the bars and, thus, the amount of energy dissipated during an earthquake.

The post-tensioning tendons and the mild steel bars are placed inside ducts preformed in the beam and column members as described by Stone et al.[7] and Stanton et al.[8] Each beam has a rectangular cross section at its ends and, near midspan, it has a trough at the top and bottom. During construction, the mild steel bars are placed in the trough and passed through the ducts at the end of the beam, which align with matching ducts in the column.

The bond between the post-tensioning tendons and the concrete is prevented inside the column and over a certain length at the ends of the beams to delay the yielding of the tendons and to reduce the cracking of the concrete. Similarly, the bond between the mild steel bars and the concrete may be prevented over a certain length at

the ends of the beams (by wrapping the bars) to prevent fracturing of the mild steel and reduce cracking of the concrete during the deformations of the bars in tension. Adequate anchorage is provided to the mild steel bars by grouting the ducts inside the beams and the column.

Previous experimental and analytical investigations[3,7-10] of systems similar to the system in Fig. 2 have shown that hybrid precast frames possess excellent seismic characteristics, including self-centering capability and significant energy dissipation. The results of these investigations have led to the successful development and application of guidelines for the design of hybrid precast frame structures for use in seismic regions.[11-13] Similar seismic design guidelines and recommendations are needed for hybrid precast walls.

In the hybrid precast wall system investigated in this paper, most of the mild steel reinforcement is placed near the two ends of the wall [see Fig. 1(b)] similar to the placement of the mild steel reinforcement near the top and bottom of the beams in Fig. 2. As compared with monolithic cast-in-place reinforced concrete walls with similar flexural strength and stiffness, the amount of mild steel that would be needed in a hybrid precast wall is smaller because a portion of the wall's resistance to lateral loads is provided by the post-tensioning steel.

Similar to the construction of the hybrid precast frame system described above, the mild steel bars are passed through preformed ducts in each wall panel, which align with matching ducts in the other panels and the foundation. The mild steel reinforcement is anchored to the foundation and the wall panels by grouting the ducts, and is extended a sufficient height above the base of the wall, after which it may be terminated [Fig. 1(b)].

In order to reduce cracking of the concrete and prevent fracturing of the mild steel, the bond between the steel and the concrete may be prevented over a certain height above the base-panel-to-foundation joint and at the panel-to-panel joints by wrapping the reinforcement in a manner similar to that shown in Fig. 2.

ANALYTICAL MODELING

Analytical modeling of the walls investigated in this paper is based on a previous model developed for walls without mild steel reinforcement. The previous model is described in detail by Kurama et al.[2,14] As an example, Fig. 3(a) shows the analytical model for a six-story wall. Fiber beam-column elements are used to represent the concrete wall panels, and truss elements are used to represent the unbonded post-tensioning steel. The verification of the model is described in Kurama et al.[2] and Kurama.[5]

Modeling of the Wall Panels

Each fiber beam-column element [Fig. 3(a)] modeling the wall panels consists of a number of parallel fibers in the direction of the height of the panel. The fiber elements used to model the wall panels described in Kurama et al.[2,14] do not include any steel fibers (i.e., only concrete fibers are used to model a wall panel). This is because the walls investigated by Kurama et al. do not have any bonded steel reinforcement crossing the horizontal joints to provide flexural strength to resist lateral loads.

Different from this previous model, the analytical model described in this paper includes steel fibers to represent the bonded mild steel reinforcement used in the wall panels. Similar to the previous model, the wire mesh used in the panels is not included in the fiber elements since the wire mesh is not continuous across the horizontal joints and, thus, does not contribute to the flexural strength of the wall.

Each concrete or steel fiber used in the analytical model has a location in the panel cross section, a cross-sectional area, and a uniaxial stress-strain relationship. The mild steel reinforcement is assumed to be adequately anchored and fully bonded to the concrete, ignoring any slip due to anchorage or bond failure. Thus, the strains in adjacent steel and concrete fibers (across the wall thickness) are assumed to be the same.

Typically, a larger number of fiber elements and fibers are used to model the wall panels near the base of a wall where the nonlinear behavior is expected to concentrate (as compared with the upper story wall panels). The stress-strain relationship of each fiber is a multi-linear idealization of the smooth uniaxial stress-strain relationship for either the mild steel, the spiral confined concrete, or the unconfined concrete (i.e., concrete outside the spirals) in the panels.

The assumed stress-strain relationship for the mild steel is shown in Fig. 3(b), which is based on experimental results reported by Paulay and Priestley.[15] The stress-strain relationships of the unconfined concrete [Fig. 3(c)] and the spiral confined concrete are based on a model developed by Mander et al.[16] Young's modulus for concrete, E_c, is assumed to be equal to $57{,}000\sqrt{f_c'}$ (in psi). The concrete confinement provided by the wire mesh used in the wall panels is ignored.

Modeling of the Unbonded Post-Tensioning Bars

Each unbonded post-tensioning bar in a wall is modeled using a series of truss elements connected to each other at the floor levels. The post-tensioning of the wall is simulated by initial tensile forces in the truss elements, which are equilibrated by compressive forces in the fiber elements.

At the base of the wall, the truss element nodes are assumed to be fixed to the foundation. At the top of the wall (i.e., at the roof), the truss element nodes are kinematically constrained to the fiber element node to model the anchorages between the post-tensioning bars and the wall [see Fig. 3(a)]. Thus, the horizontal, vertical, and rotational displacements of the truss element nodes at the roof are constrained to the displacements of the fiber element node at the roof.

At each floor level, the truss element nodes are kinematically constrained to the corresponding fiber element node at the same level assuming that the post-tensioning bars and the wall panels go through the same lateral displacements. Only the horizontal displacements of the truss element nodes are constrained to the displacements of the fiber element nodes at the floor levels. The vertical and rotational displacements of the truss ele-

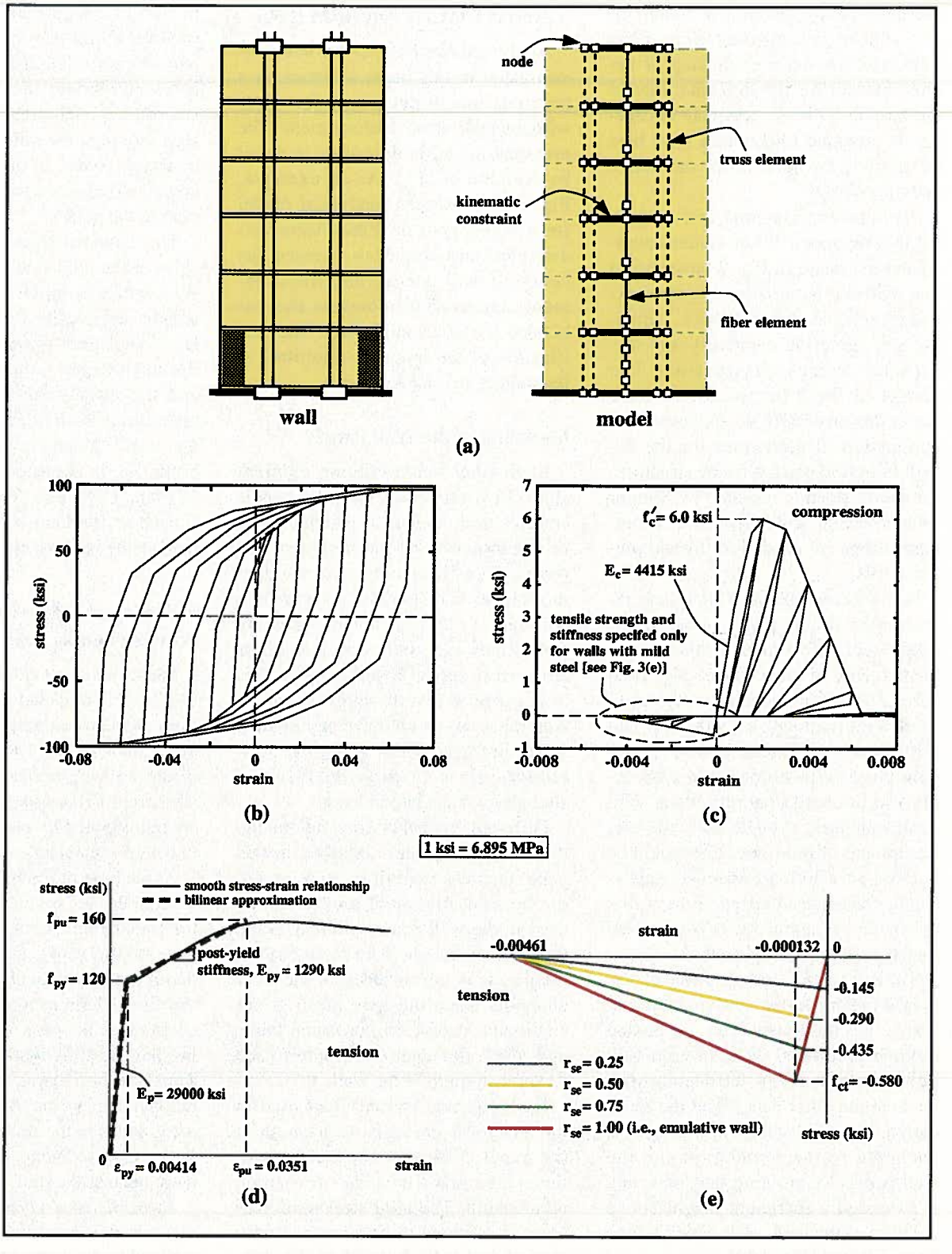

Fig. 3. Analytical model: (a) elevation; (b) mild steel; (c) unconfined concrete; (d) PT steel; (e) concrete behavior in tension.

ment nodes at the floor levels are not constrained since the post-tensioning bars are not bonded to the concrete.

The stress-strain relationship of the truss elements is a bilinear idealization of the smooth stress-strain relationship assumed for the post-tensioning steel, as shown in Fig. 3(d). The yield strength of the truss elements is assumed to be equal to the linear limit stress (i.e., stress at the limit of proportionality) of the post-tensioning steel stress-strain relationship, f_{py}.

The linear elastic stiffness of the truss elements is assumed to be equal to Young's modulus for the post-tensioning steel, E_p. The post-yield stiffness of the truss elements, E_{py}, is determined by fitting a straight line to the nonlinear portion of the post-tensioning steel stress-strain relationship between the yield stress, f_{py}, and the ultimate (i.e., peak) stress, f_{pu}. Since the steel is not bonded to the concrete,

Table 1. The prototype walls.

	High seismicity												Moderate seismicity			
	Four-story				Six-story				Ten-story				Six-story			
System	Wall	ρ_p (%)	ρ_s (%)	T (sec)	Wall	ρ_p (%)	ρ_s (%)	T (sec)	Wall	ρ_p (%)	ρ_s (%)	T (sec)	Wall	ρ_p (%)	ρ_s (%)	T (sec)
UP	PH4	1.55	0	0.48	PH6	1.44	0	0.64	PH10	1.43	0	0.99	PM6	0.41	0	0.99
HY	–	–	–	–	HH6-25	1.03	0.49	0.63	–	–	–	–	–	–	–	–
	–	–	–	–	HH6-50	0.68	0.96	0.61	–	–	–	–	HM6-50	0.22	0.32	0.98
	–	–	–	–	HH6-75	0.33	1.39	0.59	–	–	–	–	–	–	–	–
EM	EH4	0	1.94	0.43	EH6	0	1.83	0.58	EH10	0	1.88	0.89	EM6	0	0.62	0.97

Note: UP = Unbonded post-tensioned wall; HY = Hybrid wall; EM = Emulative wall.

the maximum strains in the post-tensioning bars during an earthquake are expected to remain well below the strain ε_{pu} corresponding to f_{pu} and, thus, the behavior of the post-tensioning steel beyond ε_{pu} is not modeled.

Modeling of Gap Opening

In unbonded post-tensioned precast walls without bonded mild steel reinforcement crossing the horizontal joints, the opening of discrete gaps at the joints with little or no cracking in the wall panels can occur since the post-tensioning steel is not bonded to the concrete. As a result of gap opening, large compressive stresses develop near the regions of a wall panel in contact with another panel or with the foundation (i.e., contact regions), while the tensile stresses in a significant portion of the panel are equal or close to zero.[17]

The compressive behavior of the wall panels in the contact regions is modeled using the uniaxial compressive stress-strain relationship of the concrete fibers in the fiber beam-column elements. To model the gap opening behavior in walls without mild steel reinforcement, the tensile strength and stiffness of the concrete fibers representing the wall panels are set to zero as described in Kurama et al.[2,14] and verified in Kurama.[5]

Thus, the gap opening displacements that occur at the horizontal joints are modeled as distributed tensile deformations that occur in the fiber elements over the height of the wall panels. The reduction in the flexural stiffness of a wall as a result of gap opening[1,2] is represented by the zero stiffness of the concrete fibers that go into tension when the precompression stresses due to gravity and post-tensioning forces are overcome by the flexural stresses that develop at the tension side of the wall due to lateral loads.

For walls with mild steel reinforcement crossing the horizontal joints, the opening of discrete gaps at the joints is restricted since the mild steel reinforcement is assumed fully bonded and anchored to the concrete. The steel fibers that are used to represent the bonded mild steel bars in the wall panels capture this effect in the analytical model.

While the tensile stresses in the wall panels above and below a gap at a horizontal joint are expected to remain small, significant tensile stresses may develop (and cracking may occur) in the panels away from the horizontal joint as a result of the bond between the mild steel reinforcement and the concrete. To represent these stresses, the tensile strength of concrete is considered in the modeling of the wall panels away from the horizontal joints [see Figs. 3(c) and 3(e)].

For walls with bonded mild steel reinforcement only (i.e., with no post-tensioning steel) emulating monolithic cast-in-place reinforced concrete walls, the tensile strength of concrete away from the horizontal joints, f_{ct}, is assumed to be equal to $7.5\sqrt{f_c'}$ (in psi). For walls with no mild steel (i.e., with post-tensioning steel only), representing unbonded post-tensioned precast walls, the tensile strength of concrete is assumed to be equal to zero for the entire wall as described above.

To achieve a smooth transition between the prototype walls with mild steel only (i.e., emulative walls) and the prototype walls with no mild steel investigated in this paper, the tensile strength of concrete is assumed to decrease with the amount of mild steel used in the walls as shown in Fig. 3(e).

In Fig. 3(e), the amount of mild steel used in the hybrid walls divided by the amount of mild steel used in the emulative walls is referred to as r_{se}. For example, for a hybrid system with one-half the amount of mild steel reinforcement used in the emulative system (i.e., $r_{se} = 0.50$), the tensile strength of concrete is assumed to be equal to $0.5f_{ct} = 3.75\sqrt{f_c'}$.

Advantages and Limitations of the Analytical Model

A significant advantage of using fiber beam-column elements for the wall panels is that a reasonably accurate model can be developed using only uniaxial stress-strain models for the concrete, mild steel, and post-tensioning steel, and the dimensions of the wall. The model, referred to as the fiber wall model, accounts for the axial-flexural interaction in the wall, the gap opening along the horizontal joints, and the hysteretic behavior of the mild steel, post-tensioning steel, spiral confined concrete, and unconfined concrete (including cracking and crushing of concrete). Note that buckling and low cycle fatigue fracture of the mild steel bars are not modeled.

The degradation (if any) in the flexural stiffness and resistance of the walls due to increasing lateral displacements is modeled; however, any additional degradation under repeated displacement cycles to a constant amplitude is not captured.

As described in detail by Kurama et al.,[1,2] the desired behavior of unbonded post-tensioned precast walls under lateral loads is governed, primarily, by the opening of gaps along the horizontal joints and, to a smaller extent, by the axial-flexural deforma-

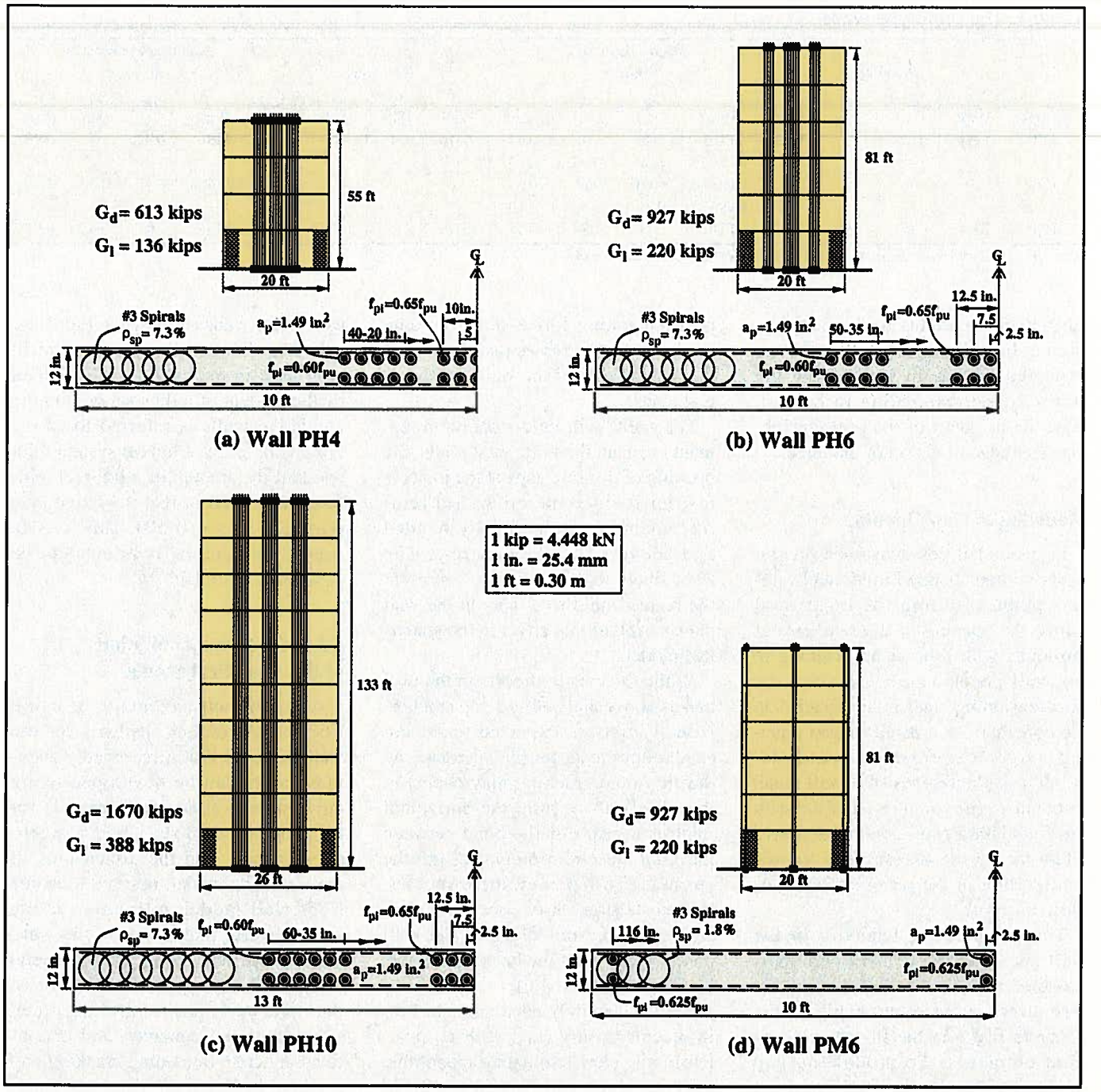

Fig. 4. Elevation and cross section (half wall length near base) of unbonded post-tensioned walls: (a) PH4; (b) PH6; (c) PH10; (d) PM6.

tions of the wall panels. Shear slip along the horizontal joints of the walls is not desired and is prevented by design,[1] because there is no restoring force to control and reverse the shear slip displacements that may occur during an earthquake. Therefore, shear slip behavior between the wall panels and between the base panel and the foundation of the prototype walls investigated in this paper is not expected and is not modeled.

The fiber wall model accounts for the linear and nonlinear axial-flexural (including gap opening) deformations and linear shear deformations of the wall panels under lateral loads; however, nonlinear shear deformations of the wall panels are not modeled. The nonlinear shear deformations of the wall panels may be significant, depending on the wall height-to-length aspect ratio, especially for walls with significant amounts of bonded mild steel reinforcement restricting gap opening behavior (e.g., the emulative walls).

According to Paulay and Priestley,[15] shear deformations in monolithic cast-in-place reinforced concrete walls with aspect ratios smaller than 4.0 may need to be considered in seismic analysis and design. The aspect ratios of the four-, six-, and ten-story prototype walls investigated in this paper (described below) are 2.8, 4.1, and 5.1, respectively. Thus, shear deformations of the wall panels may play an important role in the seismic behavior of the four-story prototype

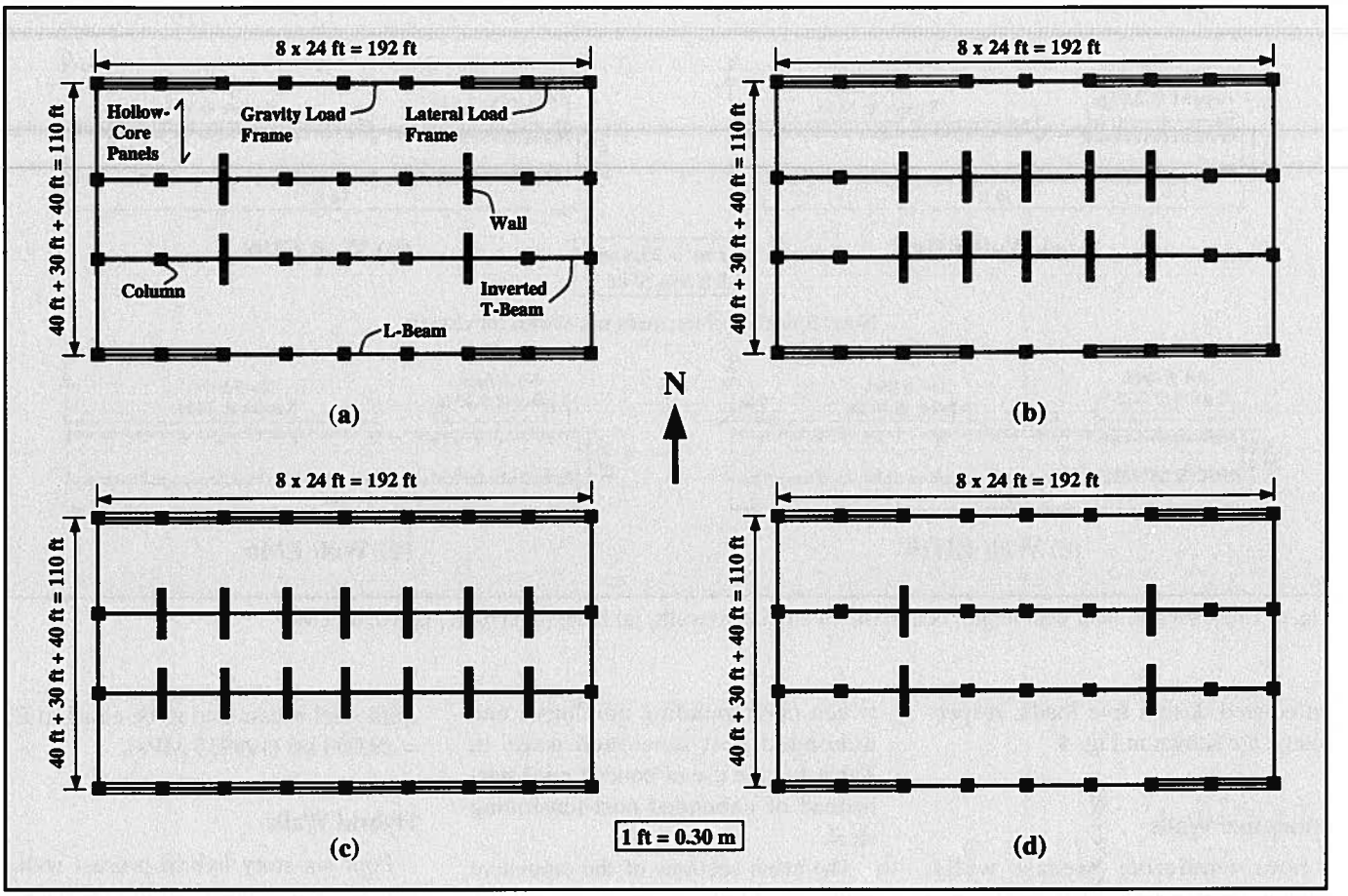

Fig. 5. Plan view of prototype buildings: (a) four-story, high seismicity; (b) six-story, high seismicity; (c) ten-story, high seismicity; (d) six-story, moderate seismicity.

walls. It is recommended that the results presented below for the four-story walls be used with caution, keeping in mind that the nonlinear shear deformations of the wall panels were not modeled.

The foundations for the walls are assumed to be fixed to the ground, ignoring any soil-structure interaction that may occur during an earthquake.

THE PROTOTYPE WALLS

This section describes the prototype walls that are investigated in this paper. A total of four unbonded post-tensioned walls, four walls that emulate the behavior of monolithic cast-in-place reinforced concrete walls under lateral loads (referred to as emulative walls), and four hybrid walls are considered as follows (see Table 1).

Unbonded Post-Tensioned Walls

The prototype unbonded post-tensioned precast concrete walls were designed using the procedure described by Kurama et al.[1,2] and the provisions of IBC-2000.[18] A total of four walls were designed as follows:

1. Wall PH4: a four-story wall for a region with high seismicity (e.g., coastal California).
2. Wall PH6: a six-story wall for a region with high seismicity.
3. Wall PH10: a ten-story wall for a region with high seismicity.
4. Wall PM6: a six-story wall for a region with moderate seismicity (e.g., Boston, Massachusetts).

The walls were designed for a site with a "medium" soil profile (Site Class D) using a response modification coefficient of $R = 5$ as recommended in IBC-2000 for special reinforced concrete bearing shear walls. The elevation and cross section views of the walls and the plan views of the office buildings for which the walls were designed are shown in Figs. 4 and 5, respectively.

It is assumed that the walls provide the entire lateral load resistance in the north-south direction of the prototype buildings. The lateral load resisting frames in the east-west direction of the buildings are not addressed in this paper.

The total area of the post-tensioning steel as a percentage of the gross cross-sectional area of each prototype wall (referred to as the post-tensioning steel ratio, ρ_p) is given in Table 1. The assumed design properties of the concrete and post-tensioning steel are shown in Figs. 3(c) and 3(d), respectively.

The compressive strength of unconfined concrete is assumed to be equal to f'_c = 6.0 ksi (41.4 MPa). The yield strength and ultimate strength of the post-tensioning steel are assumed to be equal to f_{py} = 120 ksi (827 MPa) and f_{pu} = 160 ksi (1103 MPa), respectively, as shown in Fig. 3(d). Young's modulus for the post-tensioning steel is assumed to be equal to E_p = 29,000 ksi (199955 MPa).

The axial forces near the base of the walls, G_d and G_l, due to the unfactored design dead loads and the unfactored

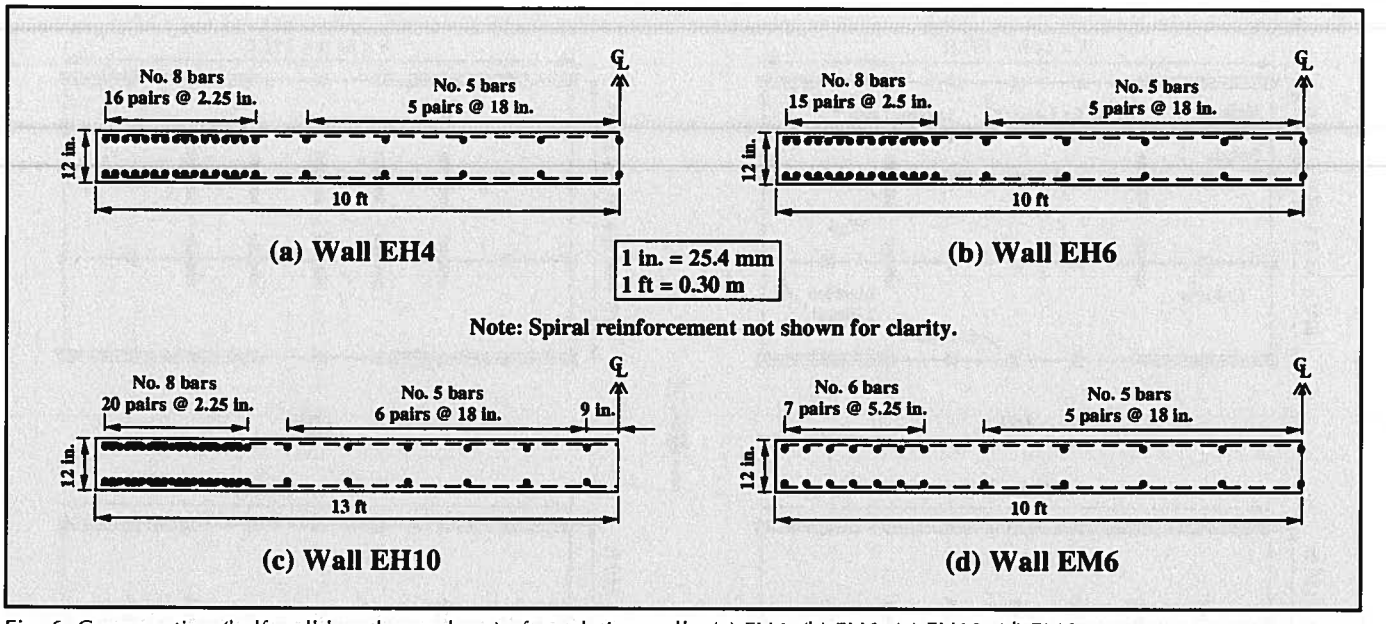

Fig. 6. Cross section (half wall length near base) of emulative walls: (a) EH4; (b) EH6; (c) EH10; (d) EM6.

unreduced design live loads, respectively, are shown in Fig. 4.

Emulative Walls

Four emulative precast walls, namely, Walls EH4, EH6, EH10, and EM6, were determined using the four unbonded post-tensioned precast Walls PH4, PH6, PH10, and PM6, respectively, described above.

One of the objectives of this paper is to compare the expected seismic behavior of walls with similar flexural strengths and initial stiffnesses (and, thus, similar linear elastic fundamental periods), but with different amounts of energy dissipation. Thus, the emulative walls investigated in the paper were determined by replacing the unbonded post-tensioning steel in the unbonded post-tensioned walls with a sufficient amount of bonded mild steel reinforcement to result in similar flexural strengths to resist lateral loads.

Note that there may be other methods to emulate the behavior of monolithic cast-in-place reinforced concrete walls, such as by using ductile connectors along the horizontal joints between the wall panels and between the wall and the foundation. These types of walls are not considered in this paper since the main focus of the research is to investigate the use of mild steel reinforcement in the walls. Thus, the only significant difference between corresponding emulative and unbonded post-tensioned walls in Table 1 is the use of bonded mild steel instead of unbonded post-tensioning steel.

The cross sections of the emulative walls are shown in Fig. 6 (for clarity, the spiral reinforcement used near the base of the walls is not shown). The total area of the mild steel reinforcement as a percentage of the gross cross-sectional area of each prototype wall (referred to as the mild steel ratio, ρ_s) is given in Table 1.

A nominal amount of mild steel (ρ_s = 0.25 percent) is distributed at 18 in. (457 mm) spacing within approximately 70 percent of the wall length in the middle. The remainder of the mild steel is distributed at a reduced spacing within approximately 15 percent of the wall length near each end. To simplify the analysis of the prototype walls, the mild steel reinforcement is assumed to extend over the entire wall height. In practice, the reinforcement may be terminated at a sufficient height above the base of the wall; however, this is not investigated in this paper.

The yield strength and ultimate strength of the mild steel are assumed to be equal to f_{sy} = 60 ksi (414 MPa) and f_{su} = 97 ksi (669 MPa), respectively, with the ultimate strength reached at a strain of 0.06 as shown in Fig. 3(b). Young's modulus for the mild steel is assumed to be equal to E_s = 29,000 ksi (199955 MPa).

Hybrid Walls

Four six-story hybrid precast walls are considered based on the unbonded post-tensioned walls and the emulative walls described above. Hybrid Walls HH6-25, HH6-50, and HH6-75 have, approximately, 0.25, 0.50, and 0.75 times, respectively, the amount of mild steel reinforcement used in Wall EH6 for a region with high seismicity. Similarly, Wall HM6-50 has, approximately, 0.50 times the amount of mild steel reinforcement used in Wall EM6 for a region with moderate seismicity.

The amount of the post-tensioning steel used in the hybrid walls was determined so as to result in similar flexural strengths as Walls PH6 and PM6 for regions with high and moderate seismicity, respectively. The cross sections of the hybrid walls are shown in Fig. 7 (for clarity, the spiral reinforcement used near the base of the walls is not shown). The post-tensioning steel ratio, ρ_p, and the mild steel ratio, ρ_s, of the walls are given in Table 1.

BEHAVIOR OF THE WALLS UNDER LATERAL LOADING

Figs. 8 to 10 show the expected base shear versus roof drift (V-Δ) behavior

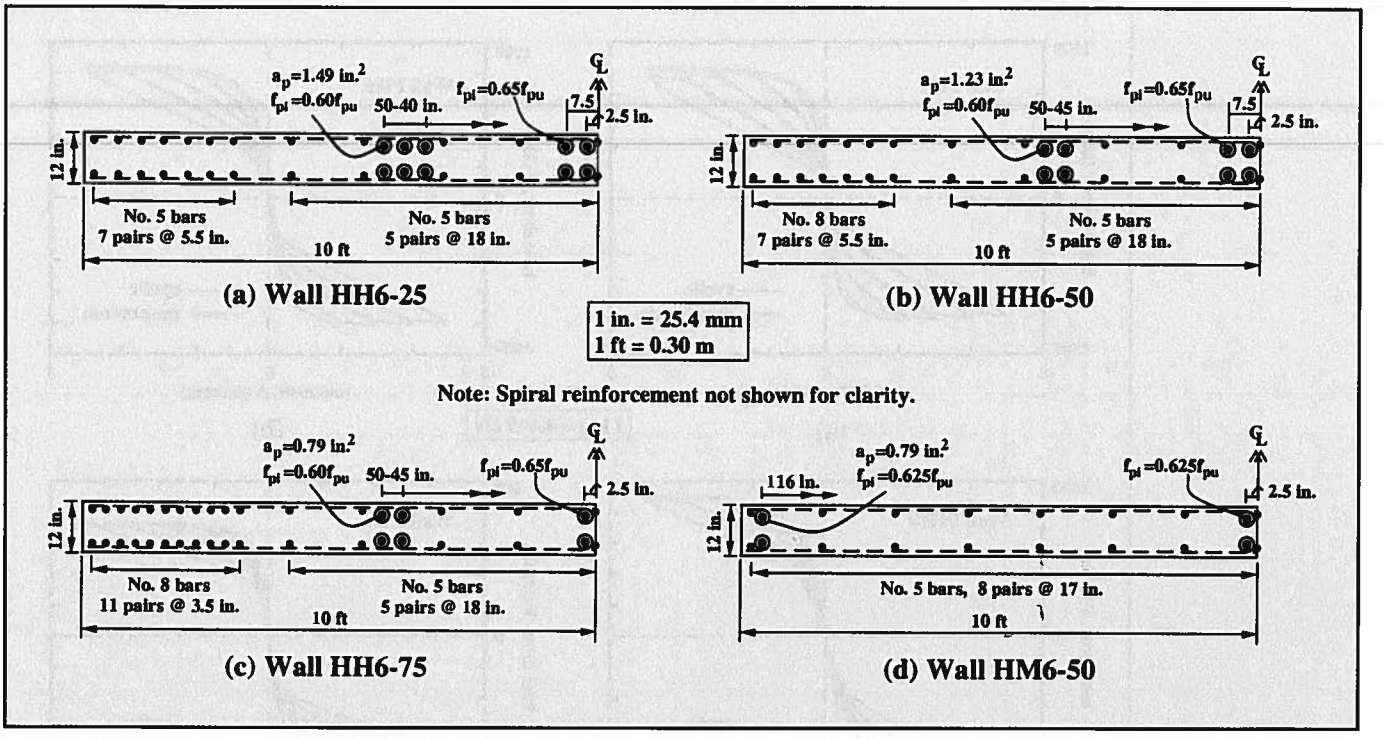

Fig. 7. Cross section (half wall length near base) of hybrid walls: (a) HH6-25; (b) HH6-50; (c) HH6-75; (d) HM6-50.

of the prototype walls under combined gravity loads and reversed cyclic lateral loads. The gravity loads acting on each wall are assumed to be equal to $1.00D + 0.25L$, where D and L are the unfactored design dead load and the unfactored unreduced design live load, respectively. This combination of dead and live loads is assumed to represent the amount of gravity load that may be acting on the walls during an earthquake.

The base shear, V, is equal to the sum of the lateral forces applied at the floor and roof levels, and the roof drift, Δ, is equal to the lateral displacement at the roof level divided by the wall height. The distribution of the lateral forces over the height of the walls is assumed to be the same as the distribution of inertial forces corresponding to the fundamental (i.e., first) mode of vibration from a linear elastic modal analysis of each structure. Note that inertial force distributions significantly different than the assumed fundamental mode distribution over the height of the walls are possible during a large earthquake (e.g., close to a uniform distribution); however, this is not investigated in this paper.

Fig. 8 shows the base shear versus roof drift relationships of the prototype unbonded post-tensioned Walls PH4, PH6, PH10, and PM6. The behavior of the walls is nearly nonlinear elastic, characterized by loading and unloading hysteresis curves that are very close to each other. The extremely narrow hysteresis loops show that the inelastic energy dissipation of the walls is small. A detailed investigation of the behavior of walls similar to the prototype unbonded post-tensioned walls in this paper can be found in Kurama et al.[1,2]

Similarly, Fig. 9 shows the base shear versus roof drift relationships of the prototype emulative Walls EH4, EH6, EH10, and EM6. The hysteretic behavior of the walls resemble the expected behavior of flexural monolithic cast-in-place reinforced concrete walls with slightly pinched hysteresis loops and considerable energy dissipation.[19-22] There are two important differences in the behavior of the prototype emulative and unbonded post-tensioned walls under cyclic lateral loading:

1. The emulative walls have much fuller hysteresis loops, indicating significantly larger inelastic energy dissipation.

2. The emulative walls have less self-centering capability, indicating the possibility of larger residual (i.e., permanent) lateral displacements after an earthquake.

Note that Wall EM6 [Fig. 9(d)], which was designed for a region with moderate seismicity, has a smaller amount of inelastic energy dissipation and a larger amount of self-centering capability than Wall EH6 [Fig. 9(b)], which was designed for a region with high seismicity. This is because the amount of mild steel reinforcement in Wall EM6 (ρ_s = 0.61 percent) is about one-third the amount of mild steel reinforcement in Wall EH6 (ρ_s = 1.88 percent), whereas, as shown in Fig. 4, the axial force near the base of Wall EM6 due to the design gravity load is the same as that of Wall EH6 (see values for G_d and G_l). The restoring effect of the gravity load in Wall EM6 is large enough to provide a significant self-centering capability to the wall.

Fig. 10 shows the base shear versus roof drift relationships of the prototype hybrid Walls HH6-25, HH6-50, HH6-75, and HM6-50. As expected, an increase in the amount of mild steel reinforcement results in an increase in the amount of energy dissipation of the walls.

The thick red lines in Figs. 8 to 10 show the base shear versus roof drift behavior of the prototype walls under

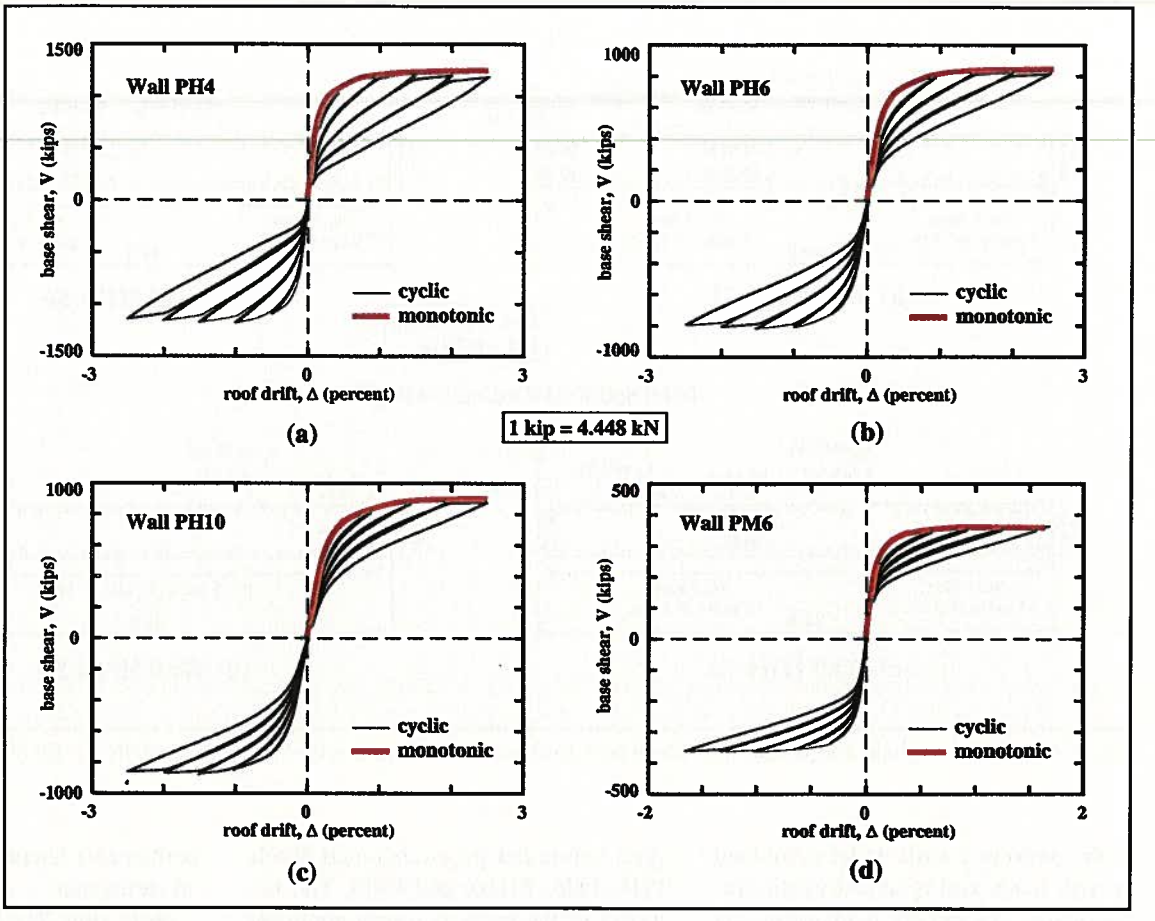

Fig. 8. Behavior of unbonded post-tensioned walls under lateral loads: (a) PH4; (b) PH6; (c) PH10; (d) PM6.

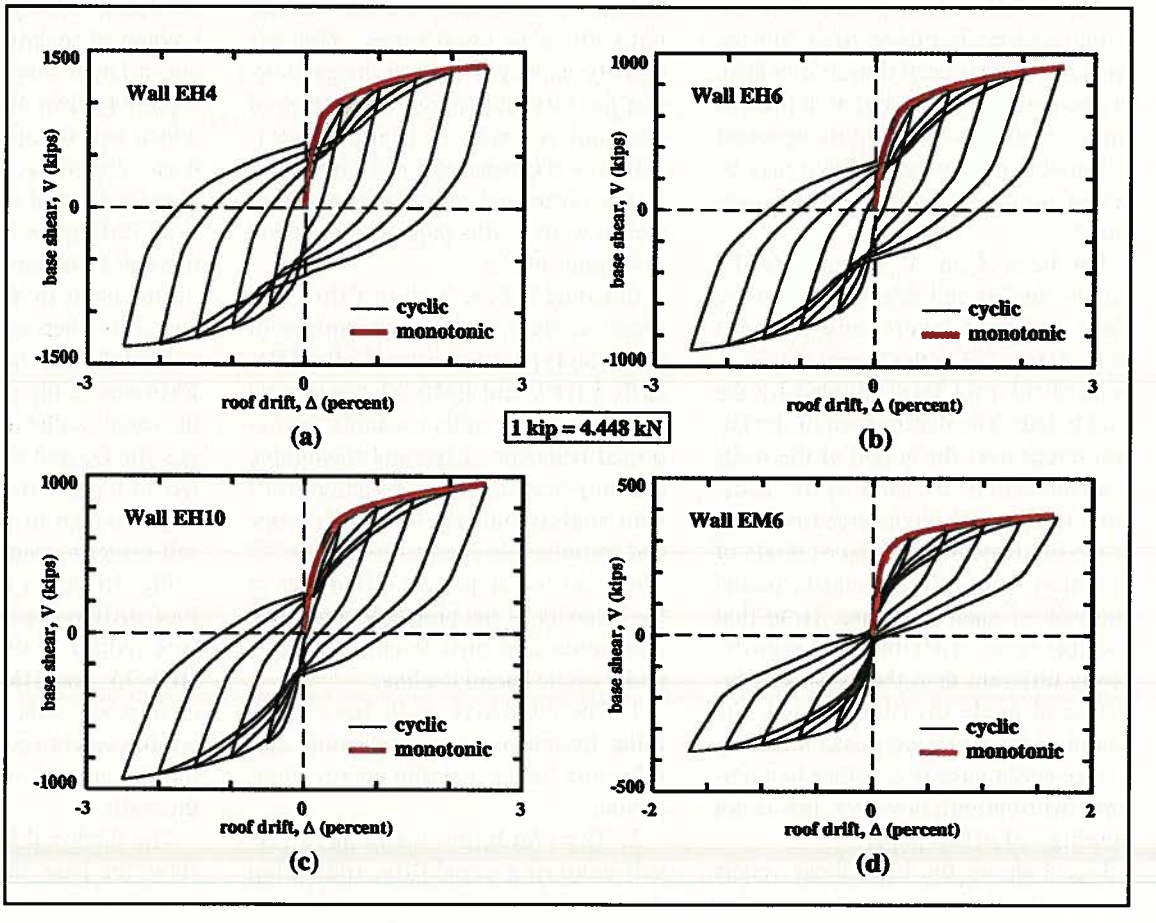

Fig. 9. Behavior of emulative walls under lateral loads: (a) EH4; (b) EH6; (c) EH10; (d) EM6.

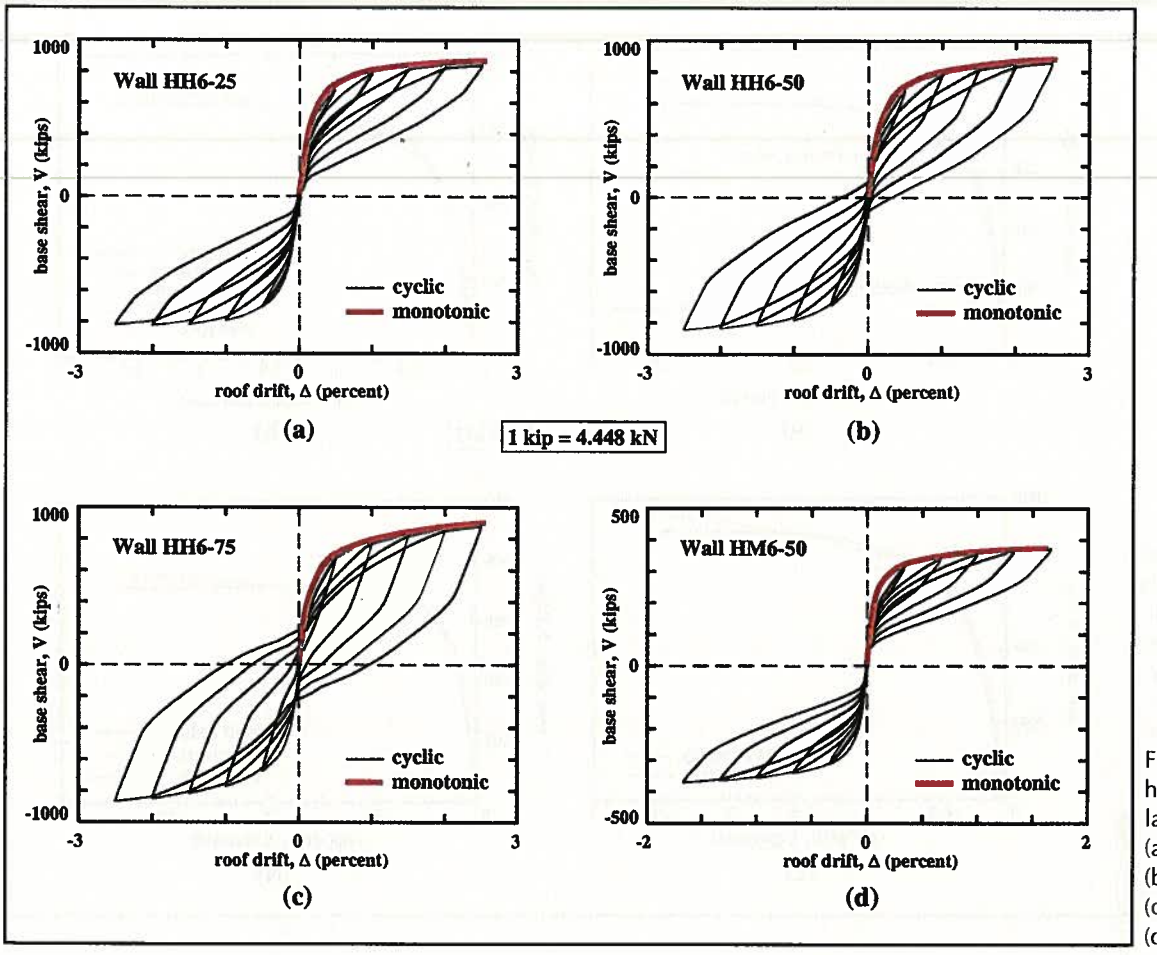

Fig. 10. Behavior of hybrid walls under lateral loads: (a) HH6-25; (b) HH6-50; (c) HH6-75; (d) HM6-50.

combined gravity loads and monotonic lateral loads as obtained from static push-over analyses. Fig. 11 provides comparisons between the push-over analysis results of corresponding unbonded post-tensioned, hybrid, and emulative walls.

Figs. 8 to 11 show that the differences in the behavior of the walls under monotonic lateral loading are insignificant as compared to the differences under cyclic lateral loading. The small differences in the behavior of the walls under monotonic lateral loading occur for two principal reasons:

1. The total post-tensioning force in a wall decreases as the area of the post-tensioning steel is decreased (since the initial stress in the post-tensioning steel, f_{pi}, is not varied as shown in Figs. 4 and 7). This results in an earlier reduction in the flexural stiffness (i.e., earlier softening) of the wall due to earlier gap opening along the horizontal joints under lateral loads.[2]

2. As shown in Table 1, the total area of the flexural steel (i.e., area of the post-tensioning steel plus area of the mild steel) in a wall increases as the post-tensioning steel is replaced with mild steel while keeping the flexural strength of the wall constant (since mild steel has significantly lower tensile strength than post-tensioning steel). This increase in the total steel area results in an increase in the flexural stiffness of the wall. Note that, as shown in Fig. 11, the effect of the steel area on the wall stiffness is greater after the opening of gaps along the horizontal joints (i.e., the post-softening range), since the flexural stiffness before gap opening (i.e., the pre-softening range) is governed by the gross cross section of the wall.

The most significant effect of the different amounts of mild steel and post-tensioning steel on the behavior of the walls under lateral loading is in the shape of the hysteresis loops and the amount of inelastic energy dissipation per cycle of loading. This is discussed in more detail below.

Inelastic Energy Dissipation

This section investigates the inelastic energy dissipation of the prototype walls based on the reversed cyclic lateral load analysis results in Figs. 8 to 10. For this purpose, the inelastic energy dissipation per loading cycle, D_h, is calculated as the area enclosed by the base shear versus roof drift relationship during that cycle. As an example, the shaded region in Fig. 12(a) is used to determine D_h for the last loading cycle (to $\pm\Delta_c = \pm 2.5$ percent, where Δ_c is the maximum roof drift reached during the cycle) of Wall EH6 in Fig. 9(b).

The inelastic energy dissipation per cycle, D_h, is normalized with the energy absorbed by an "equivalent" linear elastic system, U_e, which is equal to the sum of the hatched triangular areas in Fig. 12(a). As described in Kurama[4] and IBC-2000,[18] the normalized inelastic energy dissipation, $d_h = D_h/U_e$, is a measure of the amount of viscous damping in the equivalent linear elastic system that would result in

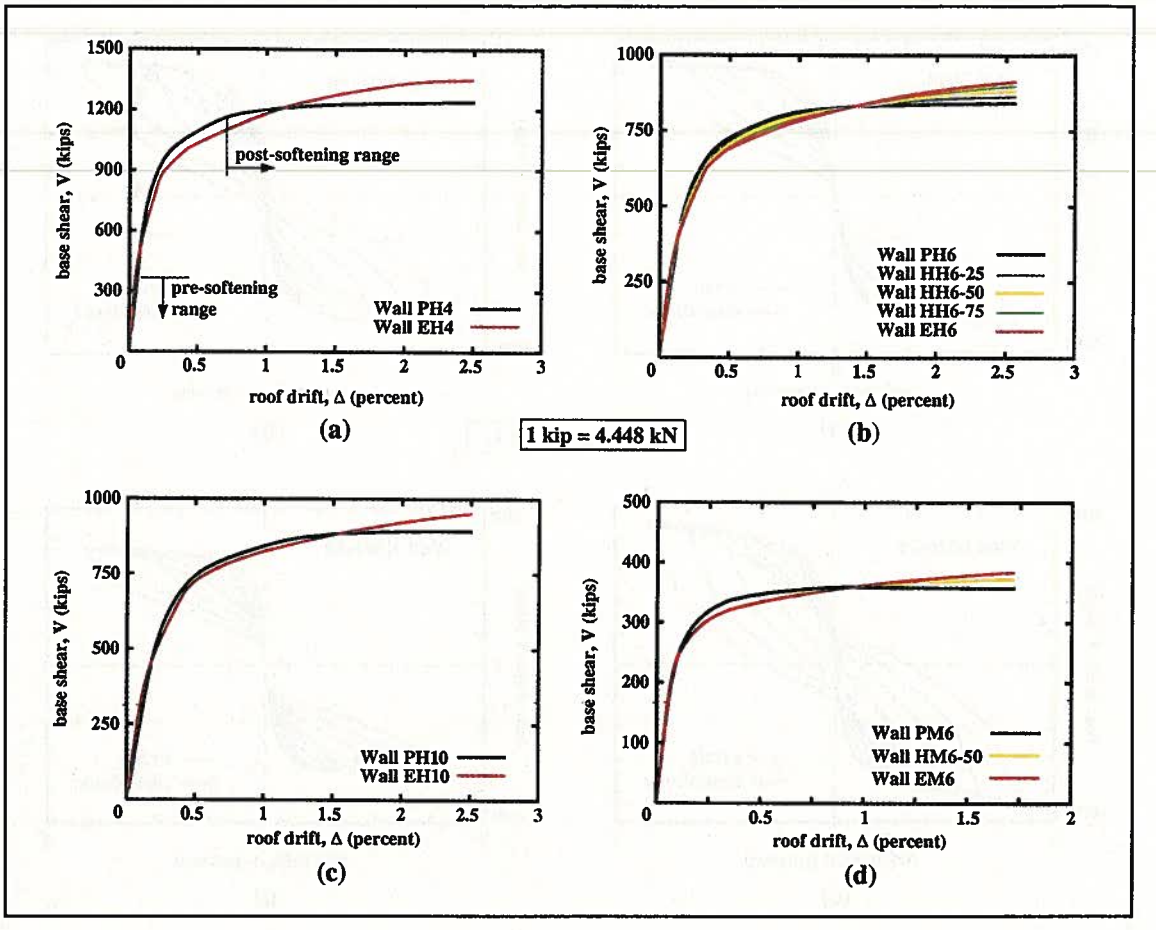

Fig. 11. Behavior of prototype walls under monotonic loading: (a) four-story, high seismicity; (b) six-story, high seismicity; (c) ten-story, high seismicity; (d) six-story, moderate seismicity.

the same amount of energy dissipation as the nonlinear system.

Note that the behavior of the prototype walls is symmetric in the positive and negative directions of loading and, thus, the amount of energy absorbed by the equivalent linear elastic system in the positive direction is the same as the energy absorbed in the negative direction. The stiffness of the equivalent linear elastic system is assumed to be the same as the secant stiffness, k_{sec}, corresponding to the maximum positive and negative roof drift reached during the cycle, $\pm\Delta_c$.

The normalized inelastic energy dissipation, d_h, of the four-story, six-story, and ten-story prototype walls in regions with high seismicity and the six-story walls in regions with moderate seismicity are shown in Figs. 12(b) to 12(e), respectively. The horizontal axes show the maximum roof drift reached during each loading cycle, Δ_c. The walls for regions with high seismicity are displaced to roof drift values of $\pm\Delta_c$ = ±0.5, ±1.0, ±1.5, ±2.0, and ±2.5 percent during each cycle and the walls for regions with moderate seismicity are displaced to roof drift values of $\pm\Delta_c$ = ±0.3, ±0.7, ±1.0, ±1.3, and ±1.7 percent (see Figs. 8 to 10).

Table 2 gives the normalized energy dissipation of the hybrid and emulative walls divided by the normalized energy dissipation of the corresponding unbonded post-tensioned walls, $r_{hp} = d_h/d_{hp}$, during the first four roof drift cycles (i.e., $r_{hp,1}$ to $r_{hp,4}$ in Table 2).

The results in Table 2 show that the inelastic energy dissipation of the walls is significantly increased as a result of the use of mild steel reinforcement. For the six-story walls in regions with high seismicity, the energy dissipation of the unbonded post-tensioned Wall PH6 can be increased to over two, three, and four times by providing 0.25, 0.50, and 0.75 times the amount of mild steel used in the emulative Wall EH6, respectively. The energy dissipation of the emulative wall is over five times that of the unbonded post-tensioned wall.

A similar measure of inelastic energy dissipation is defined using the relative energy dissipation ratio, β, in the ACI Standard and Commentary "Acceptance Criteria for Moment Frames Based on Structural Testing" (T1.1-01 and T1.1R-01).[23] It can be shown that the relative energy dissipation ratio, β, is equal to $^1/_4$ times the normalized inelastic energy dissipation, d_h, defined above.

In the ACI Standard T1.1-01,[23] the smallest acceptable value of β is specified as 0.125, which corresponds to a value of 0.5 for d_h. The ACI Standard recommends that if β is smaller than 0.125, there may be inadequate damping for the frame as a whole, and the oscillations of the frame may continue for a considerable time after an earthquake, possibly producing low-cycle fatigue effects and excessive displacements.

Similar guidelines on the required amount of energy dissipation need to be developed for precast concrete wall systems. In the absence of these guidelines, the shaded regions in Figs. 12(b) to 12(e) show the cases for which $d_h \geq 0.5$ for the prototype walls. For a wide

Table 2. Normalized energy dissipation.

High seismicity															Moderate seismicity				
Four-story					Six-story					Ten-story					Six-story				
Wall	$r_{hp,1}$	$r_{hp,2}$	$r_{hp,3}$	$r_{hp,4}$	Wall	$r_{hp,1}$	$r_{hp,2}$	$r_{hp,3}$	$r_{hp,4}$	Wall	$r_{hp,1}$	$r_{hp,2}$	$r_{hp,3}$	$r_{hp,4}$	Wall	$r_{hp,1}$	$r_{hp,2}$	$r_{hp,3}$	$r_{hp,4}$
PH4	1.00	1.00	1.00	1.00	PH6	1.00	1.00	1.00	1.00	PH10	1.00	1.00	1.00	1.00	PM6	1.00	1.00	1.00	1.00
–	–	–	–	–	HH6-25	2.50	2.01	2.02	2.22	–	–	–	–	–	–	–	–	–	–
–	–	–	–	–	HH6-50	4.97	3.26	3.30	3.57	–	–	–	–	–	HM6-50	7.56	2.62	2.60	2.83
–	–	–	–	–	HH6-75	8.05	4.68	4.49	4.83	–	–	–	–	–	–	–	–	–	–
EH4	8.68	5.75	5.63	6.21	EH6	11.7	6.22	5.60	5.96	EH10	17.7	6.58	6.27	6.21	EM6	16.4	4.70	4.60	4.84

range of cases, the results suggest that it may be possible to increase the d_h values of unbonded post-tensioned precast walls in regions with high seismicity to 0.5 by providing at least 0.50 times the amount of mild steel used in the corresponding emulative walls.

For a given target d_h value, the amount of mild steel needed (as a proportion of the amount of mild steel used in the corresponding emulative wall) increases as Δ_c decreases, the number of stories increases, or the seismicity of the region decreases.

BEHAVIOR OF THE WALLS UNDER EARTHQUAKE LOADING

In this section, the nonlinear dynamic behavior of the prototype walls under earthquake loading is examined and compared with respect to the roof drift time history, maximum roof drift, number of "large" roof drift peaks, and maximum absolute roof acceleration.

As shown in Table 1, the four-story, six-story, and ten-story walls for regions with high seismicity represent a considerable variation in the linear elastic fundamental period, T (T varies between 0.43 and 0.99 second). Thus, the effect of the fundamental period on the dynamic behavior of the walls is investigated. In addition, the effect of the seismicity of the region (i.e., high seismicity versus moderate seismicity) on the results is discussed.

The nonlinear dynamic time history analyses of the prototype walls were conducted using the fiber wall model with a time step of 0.01 second. Previous analyses[24] of similar walls show that the differences between results from analyses conducted using a time step of 0.001 second and 0.01 second are not significant. Thus, the time step of 0.01 second is adequate to capture the dynamic characteristics of the walls.

The dynamic analyses were conducted using a viscous damping ratio of $\xi = 3$ percent in the first and third linear elastic modes of vibration of the walls (using mass and stiffness proportional Rayleigh damping[25]).

The gravity loads acting on each wall were assumed to be equal to $1.00D + 0.25L$ as described earlier. The total mass of each prototype building was assumed to be distributed equally among the walls used in that building. The masses assigned to the walls were lumped at the floor and roof fiber element nodes.

Ground Motion Records

Seven ground motion records including five natural records and two artificial (i.e., generated) records (Table 3) were used in the dynamic analyses of the prototype walls. These ground motion records are considered to be representative of records on sites with a "medium" soil profile similar to the site soil condition used in the design of the prototype walls (i.e., Site Class D in IBC-2000[18]).

The ground motion records were scaled to a constant maximum incremental velocity (MIV) as described in Kurama.[5] The MIV of a ground motion is equal to the maximum area under the acceleration time history of the ground motion between two successive zero-acceleration crossings. Recent research has shown that a strong correlation exists between the MIV and the severity of a ground motion.[5,26,27]

Note that other methods of ground motion scaling based on the fundamental period of vibration of the structure have been proposed by other researchers.[27,28] The use of these scaling methods requires that different scaling factors (and, thus, different sets of scaled ground motion records) are used in the analyses of walls with different fundamental periods.

It may be desirable to use a ground motion scaling method that is independent of the structure period so that comparisons between the dynamic responses of walls with different fundamental periods can be made based on the same set of scaled ground motion records. Since MIV is a period-independent quantity,[5] the same set of scaled records are used in the analyses of the prototype walls investigated in this paper.

For regions with high seismicity, the ground motion records were scaled to an MIV value of 67 in. per second (1700 mm per second). As described in Kurama,[5] the scaled records with MIV = 67 in. per second are considered to be representative of maximum credible ground motions that can be expected in regions of the United States with high seismicity (e.g., coastal California). For regions with moderate seismicity, the ground motion records were scaled to an MIV value of 27 in. per second (690 mm per second).

More information on the ground motion records, including linear elastic single-degree-of-freedom acceleration response spectra, is given by Kurama.[5] Table 3 shows the factors that were used to scale the ground motion records, as well as the peak acceleration (PGA) and peak velocity (PGV) of the MIV-scaled records. The peak accelerations of the ground motions for regions with high seismicity vary between $0.52g$ and $1.1g$, and the peak accelerations of the ground motions for regions with moderate seismicity vary between $0.21g$ and $0.44g$, where g is the gravitational acceleration.

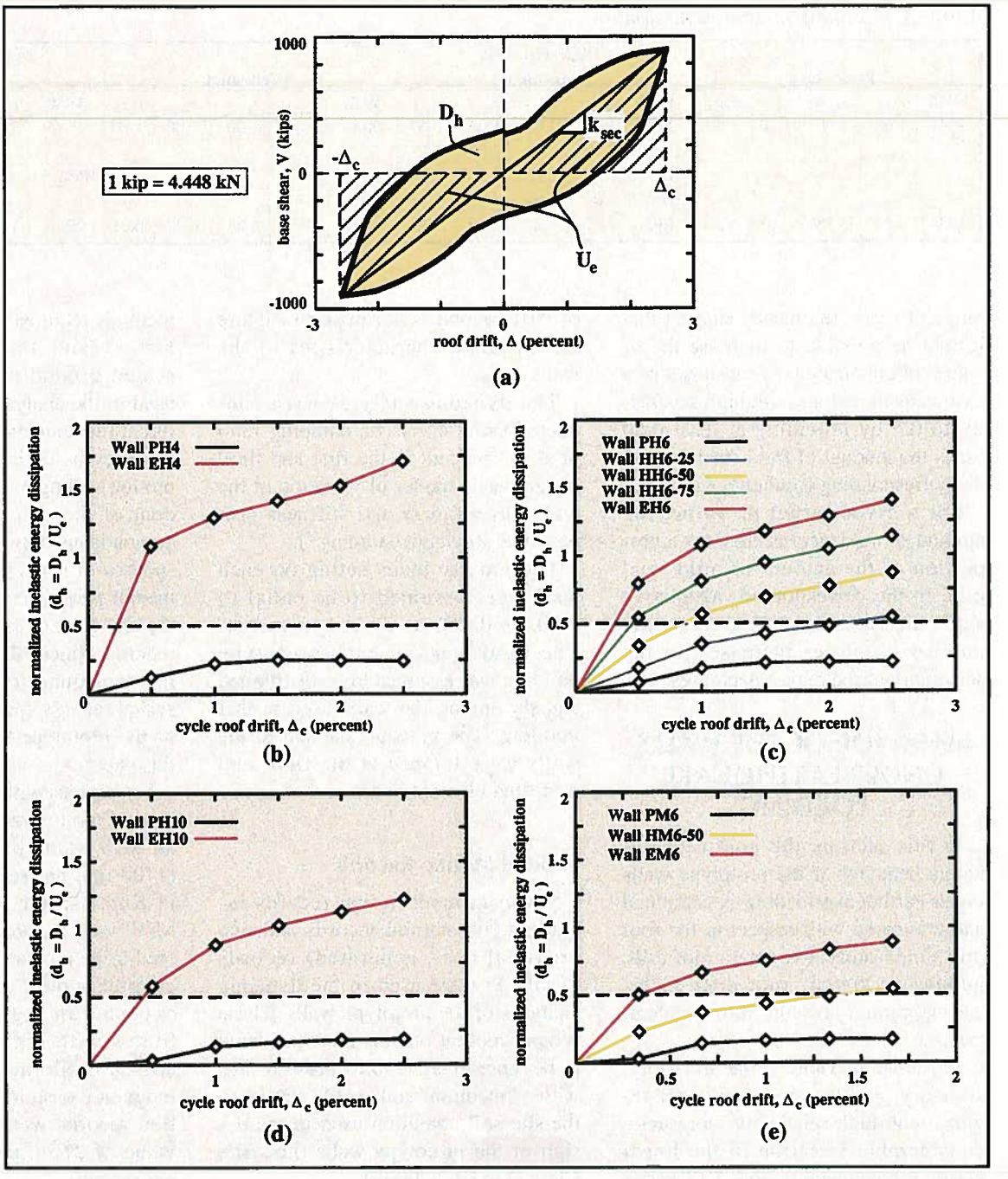

Fig. 12. Inelastic energy dissipation: (a) D_h and U_e; (b) four-story, high seismicity; (c) six-story, high seismicity; (d) ten-story, high seismicity; (e) six-story, moderate seismicity.

Roof Drift Time History Response

As examples of representative behavior, Fig. 13 shows the roof drift time histories of the prototype walls under the MIV-scaled Northridge-Sylmar (NOSY) ground motion. For regions with high seismicity [Figs. 13(a) to 13(c)], an increase in the amount of mild steel reinforcement has two important effects on the dynamic response of the walls:

1. The maximum roof drift decreases.

2. The number of large roof drift peaks decreases because the response of the wall decays faster.

These differences are, to a large extent, due to the increase in the inelastic energy dissipation of the walls as the amount of mild steel reinforcement is increased. For regions with moderate seismicity [Fig. 13(d)], the differences between the responses of the walls with different amounts of mild steel are less pronounced.

The nonlinear dynamic time history analysis results in Fig. 13 show that the amount of mild steel does not have a significant effect on the self-centering capability of the walls as indicated by the oscillations of the hybrid and emulative walls about close-to-zero drift positions.

The residual (i.e., permanent) roof drift of the prototype walls due to each ground motion was determined by conducting a free vibration analysis of each wall (i.e., by bringing each wall to "rest") after the nonlinear time history analysis under that ground motion was completed. The accelerations, velocities, and displacements, together with the stiffness properties of each wall at the end of a time history analy-

Table 3. MIV-scaled ground motion records.

Earthquake	Recording station or method of generation	High seismicity				Moderate seismicity			
		Scale factor	PGA (g)	PGV (in./sec)	MIV (in./sec)	Scale factor	PGA (g)	PGV (in./sec)	MIV (in./sec)
LPHO-Loma Prieta, 1989	Hollister-South and Pine	1.40	0.52	35	67	0.56	0.21	14	27
LAYE-Landers, 1992	Yermo-Fire Station	2.55	0.62	51	67	1.02	0.25	20	27
NONW-Northridge, 1994	Newhall-LA County Fire St.	1.11	0.66	42	67	0.44	0.26	17	27
SFOR-San Fernando, 1971	LA 8244 Orion Bl. 1st floor	3.72	0.95	44	67	1.49	0.38	18	27
NOSY-Northridge, 1994	Sylmar-County Hosp. Park.	1.15	0.97	58	67	0.46	0.39	23	27
G1M-generated[5]	SEAOC Spectrum Compatible	1.01	1.0	107	67	0.40	0.40	43	27
G2M-generated[5]	Using Kanai-Tajimi Filter	1.07	1.1	112	67	0.43	0.44	45	27

Note: 1 in. = 25.4 mm.

sis, were used as initial conditions for the subsequent free vibration analysis, which was continued until the oscillations of the wall were sufficiently small.

In general, the dynamic analyses of the prototype walls did not show significant residual drifts under the seven MIV-scaled ground motions, even for the emulative walls (the residual roof drifts for Walls EH4, EH6, EH10, and EM6 were smaller than 0.25, 0.099, 0.070, and 0.0073 percent, respectively).

Note that the small residual roof drift values obtained from the dynamic analysis results of the emulative walls are contrary to expectations, since the nonlinear static reversed cyclic analyses in Figs. 8 to 10 show that walls with larger amounts of mild steel tend to have larger amounts of residual drift upon unloading from a nonlinear lateral displacement. Furthermore, previous comparisons[1,24] between the expected dynamic responses of unbonded post-tensioned precast walls and monolithic cast-in-place reinforced concrete walls have shown significant residual drifts for the cast-in-place walls.

The differences in the estimated residual roof drift values between the previous results[1,24] and the results presented in this paper may be due to several factors, including:

1. The previous results are based on the ground motion records in Table 3 scaled to a constant peak acceleration, PGA, of 1.0g, resulting in significantly larger intensities for the LPHO, LAYE, and NONW ground motions. The largest residual drift values from the previous analyses were obtained under these records.

2. The increase in the post-softening

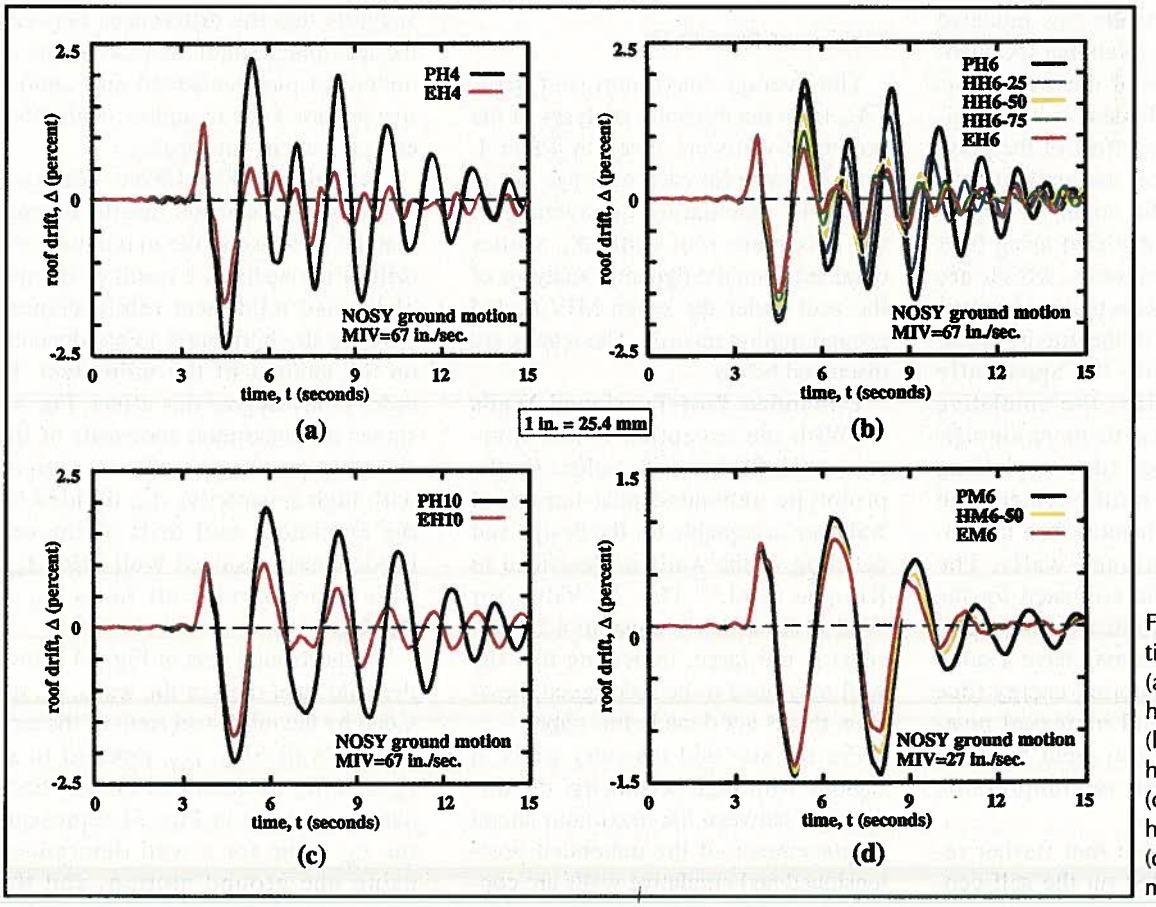

Fig. 13. Roof drift time history: (a) four-story, high seismicity; (b) six-story, high seismicity; (c) ten-story, high seismicity; (d) six-story, moderate seismicity.

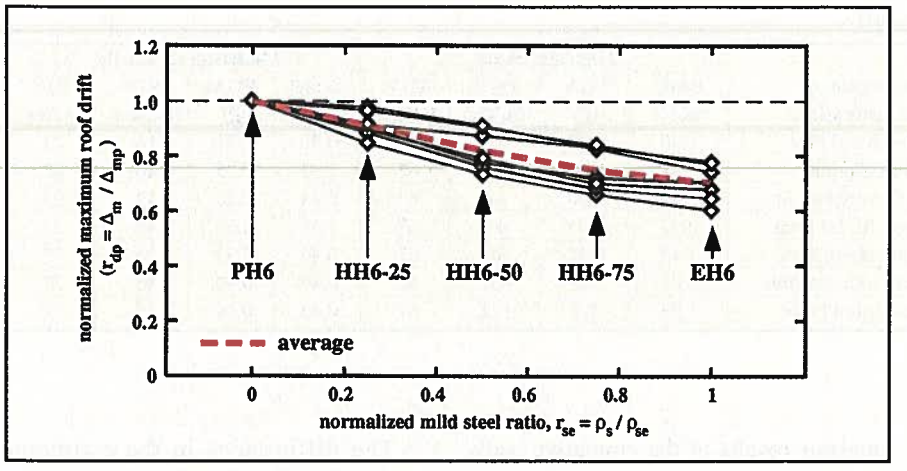

Fig. 14. Normalized maximum roof drift for the six-story walls in regions with high seismicity.

stiffness (i.e., the stiffness in the post-softening range) (see Fig. 11) of the walls as the amount of mild steel reinforcement is increased was not considered in the previous research. A larger post-softening stiffness usually results in a larger self-centering capability and, thus, a smaller residual drift since a larger amount of elastic energy is stored during the loading of the wall.[26,29]

3. In the previous research, the nonlinear behavior of the monolithic cast-in-place concrete walls was modeled using a zero-length rotational spring element[24] at the base of the walls. This rotational spring element is not sensitive to the restoring effect of the gravity loads applied on the walls. In the current research, the nonlinear behavior of the walls is modeled using fiber beam-column elements, which are axial-flexural elements that can capture the restoring effect of the gravity loads.

Note that despite the apparently small residual drifts, the emulative walls are expected to have significantly more damage (due to yielding of the mild steel reinforcement and cracking of the concrete) than the unbonded post-tensioned walls. The small residual drifts estimated for the emulative walls indicate that, upon unloading, the walls may have a sufficient amount of restoring energy (due to gravity loads and increased post-softening stiffness) to yield the mild steel reinforcement in compression and close the cracks.

It is recommended that further research be conducted on the self-centering capability of the emulative and hybrid walls. In particular, the nonlinear shear deformations of the wall panels, which may be significant for Wall EH4, were not included in the analytical model as described earlier. The lateral displacements of Wall EH4 due to the nonlinear shear deformations may be difficult to restore during and after an earthquake, resulting in larger residual drifts than estimated herein.

Maximum Roof Drift

The average maximum roof drift, $\overline{\Delta}_m$, from the dynamic analyses of the prototype walls are given in Table 4. The $\overline{\Delta}_m$ value for each wall was determined by calculating the average of the maximum roof drift, Δ_m, values obtained from the dynamic analyses of the wall under the seven MIV-scaled ground motion records. The results are discussed below.

Unbonded Post-Tensioned Walls — With the exception of the four-story Wall PH4, the $\overline{\Delta}_m$ values for the prototype unbonded post-tensioned walls are acceptable for the design and detailing of the walls as described in Kurama et al.[1,2] The $\overline{\Delta}_m$ value for Wall PH4 (which is equal to 4.21 percent) is too large, indicating that the wall may need to be redesigned; however, this is not done in this paper.

For the six- and ten-story walls in regions with high seismicity, the differences between the maximum lateral displacements of the unbonded post-tensioned and emulative walls are considerable. The maximum roof drift values of the unbonded post-tensioned Walls PH6 and PH10 are, on average, 43 and 44 percent larger than those of the corresponding emulative Walls EH6 and EH10, respectively. Note that these results are similar to previous results reported by Kurama et al.[1,24]

If desired, the maximum lateral displacements of the unbonded post-tensioned walls can be significantly reduced by using supplemental energy dissipation. For this purpose, recent research[4,5] has shown that, on average, up to 60 percent reduction in the maximum roof drift of the walls can be achieved by using supplemental friction dampers and viscous fluid dampers distributed along the height of the walls.

It may be possible to use these supplemental energy dissipation devices to reduce the maximum lateral displacements of the prototype unbonded post-tensioned Walls PH4, PH6, and PH10 to below the displacements of the corresponding emulative walls.

For regions with moderate seismicity, the maximum roof drift values of Wall PM6 are, on average, 7 percent larger than those of Wall EM6. This suggests that the differences between the maximum lateral displacements of unbonded post-tensioned and emulative precast walls in regions with moderate seismicity are small.

Hybrid and Emulative Walls — The dynamic analysis results indicate that the decrease in the maximum roof drift of the walls as a result of the use of bonded mild steel reinforcement crossing the horizontal joints depends on the amount of the mild steel. In order to investigate this effect, Fig. 14 shows the maximum roof drift of the six-story prototype walls in regions with high seismicity, Δ_m, divided by the maximum roof drift of the unbonded post-tensioned Wall PH6, Δ_{mp}. This ratio is referred to as $r_{dp} = \Delta_m/\Delta_{mp}$.

The horizontal axis in Fig. 14 shows the mild steel ratio of the walls, ρ_s, divided by the mild steel ratio of the emulative Wall EH6, ρ_{se}, referred to as $r_{se} = \rho_s/\rho_{se}$ as described earlier. Each data marker (◊) in Fig. 14 represents the r_{dp} value for a wall determined using one ground motion, and the

Table 4. Maximum roof drift.

System	High seismicity												Moderate seismicity			
	Four-story				Six-story				Ten-story				Six-story			
	Wall	$\bar{\Delta}_m$ (percent)	$\bar{r}_{dp}$	$\bar{r}_{de}$	Wall	$\bar{\Delta}_m$ (percent)	$\bar{r}_{dp}$	$\bar{r}_{de}$	Wall	$\bar{\Delta}_m$ (percent)	$\bar{r}_{dp}$	$\bar{r}_{de}$	Wall	$\bar{\Delta}_m$ (percent)	$\bar{r}_{dp}$	$\bar{r}_{de}$
UP	PH4	4.21	1.00	2.12	PH6	2.35	1.00	1.43	PH10	2.28	1.00	1.44	PM6	1.38	1.00	1.07
HY	–	–	–	–	HH6-25	2.13	0.91	1.30	–	–	–	–	–	–	–	–
	–	–	–	–	HH6-50	1.90	0.82	1.17	–	–	–	–	HM6-50	1.34	0.97	1.03
	–	–	–	–	HH6-75	1.74	0.75	1.07	–	–	–	–	–	–	–	–
EM	EH4	1.94	0.59	1.00	EH6	1.63	0.70	1.00	EH10	1.56	0.72	1.00	EM6	1.32	0.94	1.00

Note: UP = Unbonded post-tensioned wall; HY = Hybrid wall; EM = Emulative wall.

thick dashed red line shows the average value, $\bar{r}_{dp}$, considering the seven MIV-scaled ground motions used in the dynamic analyses of the walls. The relationship between $\bar{r}_{dp}$ and r_{se} is close to linear, indicating that the reduction in the maximum roof drift is, on average, nearly proportional to the amount of mild steel.

Table 4 gives the $\bar{r}_{dp}$ values for the prototype walls investigated in this paper. The average values of the $\bar{r}_{de} = \Delta_m/\Delta_{me}$ ratio (i.e., the maximum roof drift of the walls, Δ_m, divided by the maximum roof drift of the corresponding emulative walls, Δ_{me}) are also given in Table 4.

For the six-story hybrid Walls HH6-25, HH6-50, and HH6-75 (with r_{se} = 0.25, 0.50, and 0.75, respectively), the $\bar{r}_{dp}$ values are equal to 0.91, 0.82, and 0.75, respectively, indicating reductions in the maximum lateral displacements that range, on average, between 9 and 25 percent (as compared with the displacements of the unbonded post-tensioned Wall PH6).

These displacement reductions are considerably smaller than the displacement reductions of up to 60 percent (on average) that can be achieved by using supplemental friction dampers or viscous fluid dampers distributed along the height of the walls as investigated by Kurama.[4,5] Thus, it is concluded that the use of mild steel reinforcement to reduce the lateral displacements of precast walls in seismic regions may not be as effective as the use of supplemental dampers distributed along the height.

Note, however, that the use of bonded mild steel reinforcement in a wall may be more cost effective than the use of supplemental friction dampers or viscous fluid dampers, depending on the amount of reduction needed in the displacements. A cost-benefit analysis may be needed to evaluate the different alternatives in reducing the seismic displacements of the wall to a desired target displacement level.

Table 4 shows that the $\bar{r}_{dp}$ value for Wall EH4 (with r_{se} = 1.00) is considerably smaller than the $\bar{r}_{dp}$ values for Walls EH6 and EH10. This suggests that the effectiveness of the mild steel reinforcement in reducing the maximum roof drift may be larger for short-period structures (with $T \leq$ ~0.5 second) than for medium- and long-period structures.

For Walls EH6 and EH10, the $\bar{r}_{dp}$ values are similar, indicating that the effect of the structure period on the results may be small for medium- and long-period structures (with $T >$ ~0.5 second). Note that the method used in the scaling of the ground motion records may have an influence on these findings; however, this is not investigated in this paper.

The $\bar{r}_{dp}$ value for Wall EM6 is equal to 0.94, indicating that the effect of mild steel reinforcement on the maximum roof drift of walls in regions with moderate seismicity is small.

Number of Large Roof Drift Peaks

As shown in Fig. 13, the prototype walls with bonded mild steel reinforcement crossing the horizontal joints go through significantly fewer large roof drift peaks than the walls without mild steel reinforcement. This is because the response of the walls decays faster as a result of the increased energy dissipation with the use of mild steel.

It is not desirable for a wall to undergo a large number of large drift peaks during a ground motion because this indicates that the dynamic oscillations of the wall may continue for a considerable time after the earthquake, which may lead to low-cycle fatigue effects.[23]

In order to investigate this effect, Fig. 15 shows the average number of roof drift peaks, $\bar{n}_c$, from the dynamic analyses of the prototype walls under the seven MIV-scaled ground motion records. The horizontal axes show the amplitude of the roof drift peak considered, Δ_c, divided by the amplitude of the largest peak, Δ_m (i.e., the peak corresponding to the maximum roof drift), during each ground motion. This ratio is referred to as $\delta_c = \Delta_c/\Delta_m$.

The $\bar{n}_c$ value corresponding to a δ_c value in Fig. 15 represents the average number of roof drift peaks with amplitudes greater than or equal to Δ_c during the dynamic analyses of the walls. For example, the $\bar{n}_c$ value for δ_c = 1.0 is equal to 1.0, because this corresponds to the maximum roof drift (i.e., $\Delta_c = \Delta_m$) in each dynamic analysis. Similarly, the $\bar{n}_c$ value corresponding to δ_c = 0.50 is equal to the average number of peaks (under the seven MIV-scaled ground motions) with amplitudes greater than or equal to 0.50 times the maximum roof drift during each ground motion.

The results in Fig. 15 demonstrate that the decay rate in the displacement response of the prototype walls tends to increase as the amount of mild steel is increased, particularly for walls in regions with high seismicity.

Note that these results do not include the reduction in the maximum roof drift of the walls as a result of the mild steel reinforcement. In order to examine this effect, the horizontal axes in Fig. 16 show the amplitude of the roof drift peak, Δ_c, divided by the

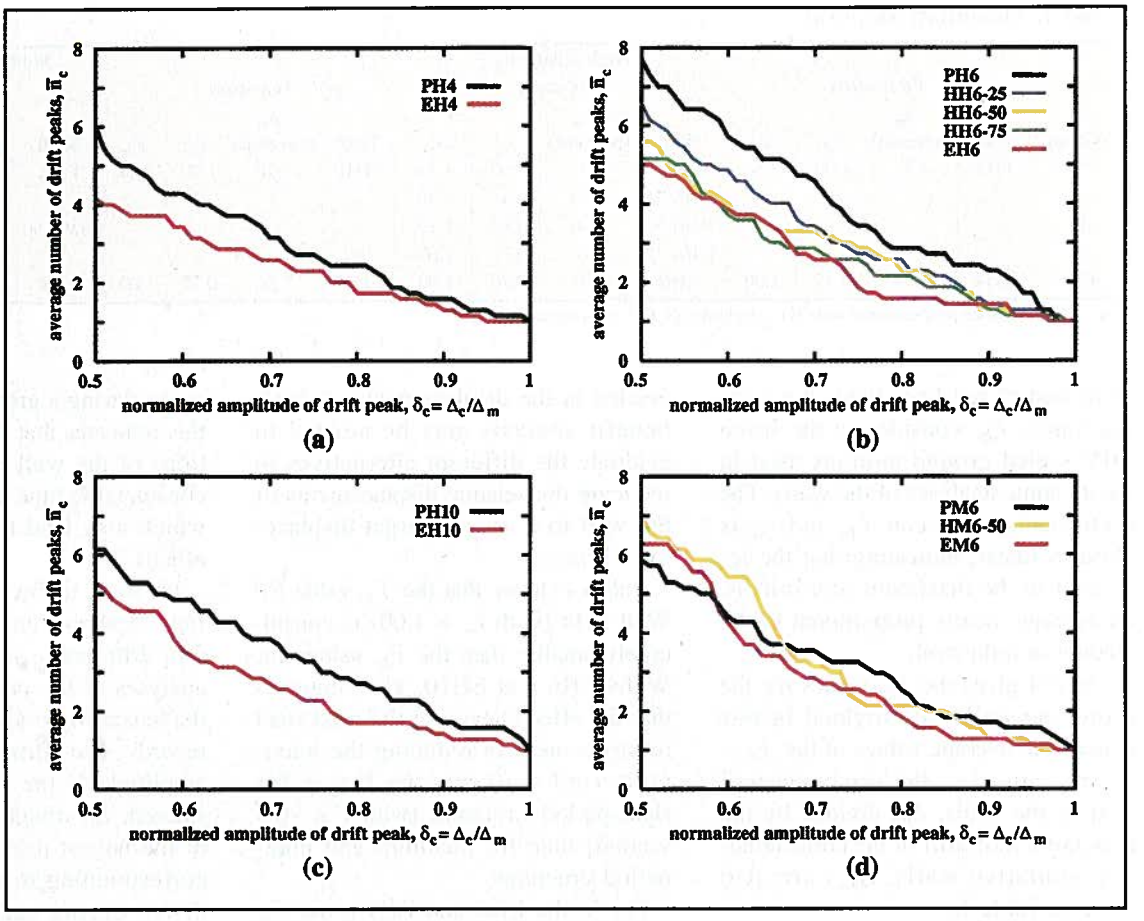

Fig. 15. $\bar{n}_c$ versus δ_c: (a) four-story, high seismicity; (b) six-story, high seismicity; (c) ten-story, high seismicity; (d) six-story, moderate seismicity.

maximum roof drift of the corresponding unbonded post-tensioned wall, Δ_{mp}, referred to as $\delta_{cp} = \Delta_c/\Delta_{mp}$. As an example, the $\bar{n}_c$ value for $\delta_{cp} = 0.50$ is equal to the average number of peaks (under the seven MIV-scaled ground motions) with amplitudes greater than or equal to 0.50 times the maximum roof drift of the corresponding unbonded post-tensioned wall during each ground motion.

Thus, Fig. 16 combines two effects of the mild steel reinforcement on the roof drift response of the walls as follows:

1. The increase in the decay rate of the response.
2. The decrease in the maximum roof drift.

The results in Fig. 16 indicate that there is a significant reduction in the number of large roof drift peaks during the time history of the prototype walls as a result of the use of the mild steel reinforcement, particularly for the walls in regions with high seismicity.

For example, the six-story hybrid and emulative Walls HH6-25, HH6-50, HH6-75, and EH6 go through, on average, 2.0, 1.0, 0.43, and 0.29 peaks, respectively, with amplitudes greater than or equal to 0.75 times the maximum roof drift of the unbonded post-tensioned Wall PH6 (i.e., $\delta_{cp} = 0.75$), whereas Wall PH6 goes through an average of 3.4 peaks [solid circular data markers in Fig. 16(b)].

In order to compare the results in Fig. 16, the number of roof drift peaks of the hybrid and emulative walls (corresponding to a δ_{cp} value) during an earthquake, n_c, is divided by the number of roof drift peaks of the corresponding unbonded post-tensioned wall, n_{cp}. This ratio is referred to as $r_{cp} = n_c/n_{cp}$. Fig. 17 shows the average value of the r_{cp} ratio, $\bar{r}_{cp}$, under the seven MIV-scaled ground motion records. The $\bar{r}_{cp}$ values for δ_{cp} equal to 0.90, 0.80, 0.70, and 0.60 are given in Table 5 ($\bar{r}_{cp,90}$ through $\bar{r}_{cp,60}$, respectively).

For example, the $\bar{r}_{cp,60}$ values for the six-story hybrid and emulative Walls HH6-25, HH6-50, HH6-75, and EH6 are equal to 0.74, 0.49, 0.36, and 0.24 [solid circular markers in Fig. 17(b)], respectively, indicating, on average, a 26, 51, 64, and 76 percent, respectively, reduction in the number of roof drift peaks with amplitudes greater than or equal to 0.60 times the maximum roof drift of the unbonded post-tensioned Wall PH6.

In general, the reduction in the number of roof drift peaks is larger for:

1. Walls with larger amounts of mild steel.
2. Walls with shorter periods of vibration.
3. Walls in regions with higher seismicity.

Fig. 17 shows that the reduction in the number of roof drift peaks tends to increase for larger δ_{cp} values. The effect of the mild steel reinforcement on the response of the walls in regions with moderate seismicity is small [see Figs. 16(d) and 17(d)].

Roof Acceleration Response

Table 6 shows the average maximum absolute roof acceleration, $\bar{a}_m$

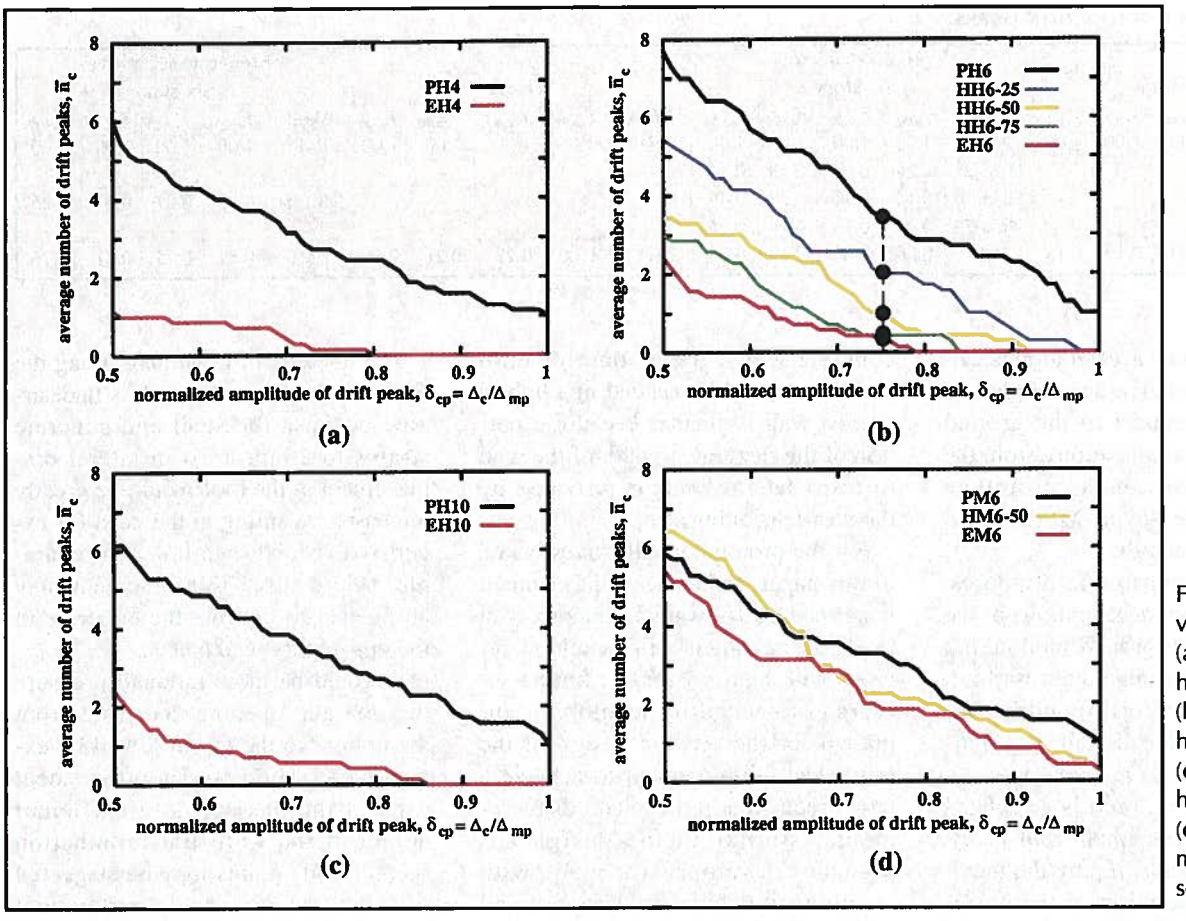

Fig. 16. $\bar{n}_c$ versus δ_{cp}: (a) four-story, high seismicity; (b) six-story, high seismicity; (c) ten-story, high seismicity; (d) six-story, moderate seismicity.

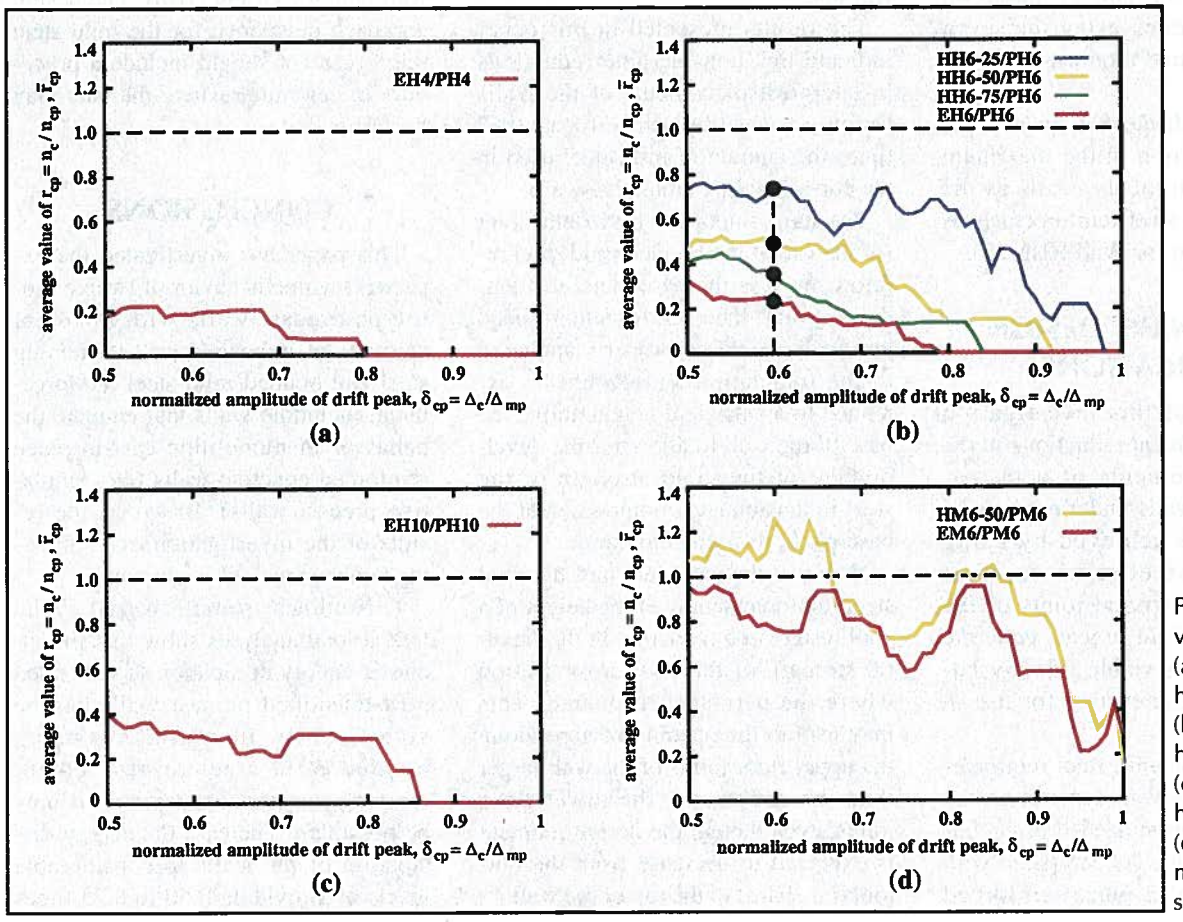

Fig. 17. $\bar{r}_{cp}$ versus δ_{cp}: (a) four-story, high seismicity; (b) six-story, high seismicity; (c) ten-story, high seismicity; (d) six-story, moderate seismicity.

Table 5. Number of roof drift peaks.

High seismicity															Moderate seismicity				
Four-story					Six-story					Ten-story					Six-story				
Wall	$\bar{r}_{cp,90}$	$\bar{r}_{cp,80}$	$\bar{r}_{cp,70}$	$\bar{r}_{cp,60}$	Wall	$\bar{r}_{cp,90}$	$\bar{r}_{cp,80}$	$\bar{r}_{cp,70}$	$\bar{r}_{cp,60}$	Wall	$\bar{r}_{cp,90}$	$\bar{r}_{cp,80}$	$\bar{r}_{cp,70}$	$\bar{r}_{cp,60}$	Wall	$\bar{r}_{cp,90}$	$\bar{r}_{cp,80}$	$\bar{r}_{cp,70}$	$\bar{r}_{cp,60}$
PH4	1.00	1.00	1.00	1.00	PH6	1.00	1.00	1.00	1.00	PH10	1.00	1.00	1.00	1.00	PM6	1.00	1.00	1.00	1.00
–	–	–	–	–	HH6-25	0.24	0.63	0.58	0.74	–	–	–	–	–	–	–	–	–	–
–	–	–	–	–	HH6-50	0.14	0.14	0.39	0.49	–	–	–	–	–	HM6-50	0.82	0.87	0.81	1.25
–	–	–	–	–	HH6-75	0.00	0.14	0.16	0.36	–	–	–	–	–	–	–	–	–	–
EH4	0.00	0.00	0.12	0.18	EH6	0.00	0.00	0.13	0.24	EH10	0.00	0.29	0.21	0.30	EM6	0.57	0.75	0.81	0.76

(where the absolute acceleration is calculated as the relative acceleration of the roof with respect to the ground plus the ground acceleration), from the dynamic analyses of the prototype walls under the seven MIV-scaled ground motion records.

In order to compare the responses, the maximum roof accelerations of the walls during each ground motion, a_m, are divided by the maximum roof acceleration of the corresponding unbonded post-tensioned wall, a_{mp}. This ratio is referred to as $r_{ap} = a_m/a_{mp}$.

Similarly, the r_{ae} ratio is calculated by dividing the maximum roof accelerations of the walls, a_m, by the maximum roof acceleration of the corresponding emulative wall, a_{me}. The average values $\bar{r}_{ap}$ and $\bar{r}_{ae}$ based on the results obtained using the seven MIV-scaled ground motions are given in Table 6.

The results indicate that, on average, there is a reduction in the maximum roof acceleration of the walls as the amount of mild steel reinforcement is increased (except for Wall HH6-25).

PRELIMINARY DESIGN IMPLICATIONS

The results of this investigation show that significant reductions in the lateral displacements of post-tensioned precast walls under earthquake loading can be achieved by using bonded mild steel reinforcement crossing the horizontal joints of the walls. Thus, hybrid precast concrete walls represent a viable primary lateral load resisting system for use in seismic regions.

The amount of mild steel reinforcement needed in a wall depends on the amount of reduction needed in the lateral displacements. As compared with monolithic cast-in-place reinforced concrete walls, the amount of mild steel that would be needed in a hybrid precast wall is smaller because a portion of the flexural strength of the wall to resist lateral loads is provided by the post-tensioning steel.

For the prototype walls investigated in this paper, mild steel reinforcement is not needed for walls in regions with moderate seismicity. For walls in regions with high seismicity, further research is needed to develop an approach for the seismic design of the mild steel reinforcement to achieve a target reduction in the lateral displacements, similar to the design approaches developed for walls with supplemental friction dampers and viscous fluid dampers as described by Kurama.[4,5]

The results presented in this paper indicate that considerable reductions in lateral displacements of the walls can be achieved by using at least 0.50 times the amount of mild steel used in the corresponding emulative wall.

The most important horizontal joint for the use of the bonded mild steel reinforcement is the base-panel-to-foundation joint. The reinforcement used in a wall should be properly anchored to the foundation and should be extended to a sufficient height above the base of the wall to allow for the development of the yield strength of the steel in tension and compression at the base-panel-to-foundation joint.

Note that the termination of the mild steel reinforcement over the height of a wall results in a reduction in the flexural strength of the wall cross section where the bars are terminated. This may lead to the opening of gaps along the upper floor joints of the wall larger than the gaps along the lower floor joints, even though the design moment is expected to decrease from the bottom (i.e., base) to the top of the wall.

The opening of large gaps along the upper floor joints of a wall is undesirable because the steel and concrete strains to attain a given lateral displacement at the roof would be greatly increased, resulting in the need for expensive special detailing. For example, heavy spiral reinforcement may be needed to confine the concrete in the upper story wall panels.

It would be more rational to ensure that the gap opening decreases from the bottom to the top of a wall by extending the mild steel reinforcement used at the base up to a sufficient height of the wall. Bar termination (i.e., cut-off) points may be staggered to achieve a reasonable curtailment pattern for the reinforcement over the wall height [see Fig. 1(b)]. The design approach developed for the mild steel reinforcement should include a procedure to determine where the bars may be terminated.

CONCLUSIONS

This paper has investigated the expected seismic behavior of twelve prototype precast walls with different amounts of unbonded post-tensioning steel and bonded mild steel reinforcement, including walls that emulate the behavior of monolithic cast-in-place reinforced concrete walls (i.e., emulative precast walls). Based on the results of the investigation, the following conclusions can be drawn:

1. Nonlinear static reversed cyclic lateral load analyses show that the inelastic energy dissipation of unbonded post-tensioned precast walls can be significantly increased by using bonded mild steel reinforcement crossing the horizontal joints. It may be possible to increase the energy dissipation of the walls to considerable levels by providing 0.50 to 0.75 times

Table 6. Maximum roof acceleration.

	High seismicity												Moderate seismicity			
	Four-story				Six-story				Ten-story				Six-story			
System	Wall	$\bar{a}_m$ (g)	$\bar{r}_{ap}$	$\bar{r}_{ae}$	Wall	$\bar{a}_m$ (g)	$\bar{r}_{ap}$	$\bar{r}_{ae}$	Wall	$\bar{a}_m$ (g)	$\bar{r}_{ap}$	$\bar{r}_{ae}$	Wall	$\bar{a}_m$ (g)	$\bar{r}_{ap}$	$\bar{r}_{ae}$
UP	PH4	1.18	1.00	1.31	PH6	1.61	1.00	1.40	PH10	1.89	1.00	1.29	PM6	0.61	1.00	1.36
HY	–	–	–	–	HH6-25	1.69	1.05	1.47	–	–	–	–	–	–	–	–
	–	–	–	–	HH6-50	1.28	0.80	1.11	–	–	–	–	HM6-50	0.53	0.90	1.22
	–	–	–	–	HH6-75	1.22	0.76	1.05	–	–	–	–	–	–	–	–
EM	EH4	0.94	0.82	1.00	EH6	1.17	0.73	1.00	EH10	1.46	0.79	1.00	EM6	0.44	0.74	1.00

Note: UP = Unbonded post-tensioned wall; HY = Hybrid wall; EM = Emulative wall.

the amount of mild steel used in the corresponding emulative walls.

2. For regions with high seismicity, the use of mild steel reinforcement has two important effects on the dynamic response of a wall under an earthquake: (1) the maximum lateral displacement of the wall decreases; and (2) the number of large displacement peaks decreases because the response of the wall decays faster.

3. For regions with moderate seismicity, the differences among the dynamic responses of unbonded post-tensioned (i.e., with post-tensioning steel only), hybrid (i.e., with post-tensioning steel and mild steel), and emulative (i.e., with mild steel only) precast walls with similar strengths and stiffnesses under lateral loads are small.

4. The use of mild steel reinforcement does not have a significant effect on the self-centering capability of the walls as indicated by the oscillations of the emulative and hybrid walls about close-to-zero displacement positions, with little residual (i.e., permanent) displacements at the end of a ground motion. This may be because of the restoring effect of the gravity loads acting on the walls and because of the increase in the "post-softening" stiffness of the walls as a result of the mild steel reinforcement.

5. With the exception of short-period walls (i.e., with linear elastic fundamental period $T \leq$ ~0.5 second), the average maximum lateral displacements of the prototype unbonded post-tensioned walls investigated in this paper are acceptable for the design and detailing of the walls.

6. For medium- and long-period walls (i.e., with $T >$ ~0.5 second) in regions with high seismicity, the maximum lateral displacements of the prototype unbonded post-tensioned walls are, on average, 40 to 45 percent larger than the displacements of the corresponding emulative walls. In regions with moderate seismicity, the differences between the maximum displacements of the unbonded post-tensioned and emulative walls are not very large (the differences are, on average, about 7 percent).

7. The amount of mild steel reinforcement needed in a wall depends on the amount of reduction needed in the lateral displacements. For the prototype walls investigated in this paper, the reduction in the maximum displacements is, on average, nearly proportional to the amount of mild steel.

Further research is needed to develop an approach for the seismic design of the mild steel reinforcement to achieve a target reduction in the lateral displacements of a wall under earthquakes. For the prototype walls in regions with high seismicity, considerable reductions in the lateral displacements can be achieved by using at least 0.50 times the amount of mild steel reinforcement used in the corresponding emulative walls.

8. The effectiveness of the mild steel reinforcement in reducing the lateral displacements of the walls may be greater for short-period structures (with $T \leq$ ~0.5 second) than for medium- and long-period structures. The effect of the structure period on the results appears to be small for medium- and long-period structures.

9. The dynamic analysis results indicate that using mild steel reinforcement to reduce lateral displacements of the walls may not be as effective as using supplemental friction or viscous fluid dampers distributed along the height of the walls as investigated by previous research.

10. On average, the maximum absolute roof accelerations of the walls tend to decrease as the amount of mild steel reinforcement is increased.

ACKNOWLEDGMENTS

This investigation is funded by the National Science Foundation (NSF) under Grant No. CMS 98-74872 as a part of the CAREER Program. The support of the NSF program directors, Dr. Shih Chi Liu and Dr. Peter Chang, is gratefully acknowledged.

The author expresses his gratitude to the PCI JOURNAL reviewers for their thoughtful and constructive comments. The guidance provided by Professor Richard Sause of Lehigh University in the conduct of the research is also gratefully acknowledged.

The opinions, findings, and conclusions expressed in this paper are those of the author and do not necessarily reflect the views of the NSF or the individuals and organizations acknowledged above.

REFERENCES

1. Kurama, Y., Pessiki, S., Sause, R., and Lu, L. W., "Seismic Behavior and Design of Unbonded Post-Tensioned Precast Concrete Walls," PCI JOURNAL, V. 44, No. 3, May-June 1999, pp. 72-89.
2. Kurama, Y., Sause, R., Pessiki, S., and Lu, L.W., "Lateral Load Behavior and Seismic Design of Unbonded Post-Tensioned Precast Concrete Walls," *ACI Structural Journal*, V. 96, No. 4, July-August 1999, pp. 622-632.
3. Priestley, M., Sritharan, S., Conley, J., and Pampanin, S., "Preliminary Results and Conclusions from the PRESSS Five-Story Precast Concrete Test Building," PCI JOURNAL, V. 44, No. 6, November-December 1999, pp. 42-67.
4. Kurama, Y., "Simplified Seismic Design Approach for Friction-Damped Unbonded Post-Tensioned Precast Concrete Walls," *ACI Structural Journal*, V. 98, No. 5, September-October 2001, pp. 705-716.
5. Kurama, Y., "Seismic Design of Unbonded Post-Tensioned Precast Walls with Supplemental Viscous Damping," *ACI Structural Journal*, V. 97, No. 4, July-August 2000, pp. 648-658.
6. Perez, F., "Lateral Load Behavior of Precast Concrete Walls with Ductile Vertical Joint Connectors," M.S. Thesis, Department of Civil and Environmental Engineering, Lehigh University, Bethlehem, PA, December 1998, 201 pp.
7. Stone, W., Cheok, G., and Stanton, J., "Performance of Hybrid Moment-Resisting Precast Beam-Column Concrete Connections Subjected to Cyclic Loading," *ACI Structural Journal*, V. 91, No. 2, March-April 1995, pp. 229-249.
8. Stanton, J., Stone, W., and Cheok, G., "A Hybrid Reinforced Precast Frame for Seismic Regions," PCI JOURNAL, V. 42, No. 2, March-April 1997, pp. 20-32.
9. Cheok, G., Stone, W., Kunnath, S., "Seismic Response of Precast Concrete Frames with Hybrid Connections," *ACI Structural Journal*, V. 95, No. 5, September-October 1998, pp. 527-539.
10. Nakaki, S. D., Stanton, J. F., and Sritharan, S., "An Overview of the PRESSS Five-Story Precast Test Building," PCI JOURNAL, V. 44, No. 2, March-April 1999, pp. 26-39.
11. Cheok, G., Stone, W., and Nakaki, S., "Simplified Design Procedure for Hybrid Precast Concrete Connections," NISTIR 5765, National Institute of Standards and Technology, Gaithersburg, MD, 1996, 81 pp.
12. ACI Innovation Task Group 1 and Collaborators, "Special Hybrid Moment Frames Composed of Discretely Jointed Precast and Post-Tensioned Concrete Members (ACI T1.2-XX) and Commentary (T1.2R-XX) (draft)," *ACI Structural Journal*, V. 98, No. 5, September-October 2001, pp. 771-784.
13. Stanton, J. and Nakaki, S., "Design Guidelines for Precast Concrete Seismic Structural Systems," PRESSS Report No. 01/03-09, UW Report No. SM 02-02, Department of Civil Engineering, University of Washington, Seattle, WA, February 2002.
14. Kurama, Y., Pessiki, S., Sause, R., Lu, L. W., and El-Sheikh., M., "Analytical Modeling and Lateral Load Behavior of Unbonded Post-Tensioned Precast Concrete Walls," Research Report No. EQ-96-02, Department of Civil and Environmental Engineering, Lehigh University, Bethlehem, PA, 1996, 191 pp.
15. Paulay, P., and Priestley, M., *Seismic Design of Reinforced Concrete and Masonry Buildings*, John Wiley & Sons, Inc., New York, NY, 1992.
16. Mander, J., Priestley, M., and Park, R., "Theoretical Stress-Strain Model for Confined Concrete," *Journal of Structural Engineering*, American Society of Civil Engineers, V. 114, No. 8, August 1988, pp. 1804-1826.
17. Allen, M., and Kurama, Y., "Design of Rectangular Openings in Precast Walls Under Combined Vertical and Lateral Loads," PCI JOURNAL, V. 47, No. 2, March-April 2002, pp. 58-83.
18. ICC, *International Building Code 2000*, International Code Council, Falls Church, VA, 2000.
19. Ali, A., and Wight, J., "Reinforced Concrete Structural Walls with Staggered Opening Configurations Under Reversed Cyclic Loading," Report No. UMCE 90-05, Department of Civil Engineering, University of Michigan, Ann Arbor, MI, April 1990, 241 pp.
20. Thomsen IV, J., and Wallace J., "Displacement-Based Design of RC Structural Walls: An Experimental Investigation of Walls with Rectangular and T-Shaped Cross-Sections," Report No. CU/CEE-95/06, Department of Civil and Environmental Engineering, Clarkson University, Potsdam, NY, June 1995.
21. Sittipunt, C., and Wood, S., "Influence of Web Reinforcement on the Cyclic Response of Structural Walls," *ACI Structural Journal*, V. 92, No. 6, November-December 1995, pp. 745-756.
22. Taylor, C., Cote, P., and Wallace, J., "Design of Slender Reinforced Concrete Walls with Openings," *ACI Structural Journal*, V. 95, No. 4, July-August 1998, pp. 420-433.
23. ACI Innovation Task Group 1 and Collaborators, "Acceptance Criteria for Moment Frames Based on Structural Testing (T1.1-01) and Commentary (T1.1R-01)," American Concrete Institute, Farmington Hills, MI, 2001, 10 pp.
24. Kurama, Y., Sause, R., Pessiki, S., Lu, L. W., and El-Sheikh, M., "Seismic Design and Response Evaluation of Unbonded Post-Tensioned Precast Concrete Walls," Research Report No. EQ-97-01, Department of Civil and Environmental Engineering, Lehigh University, Bethlehem, PA, 1997, 184 pp.
25. Clough, R., and Penzien, J., *Dynamics of Structures*, McGraw-Hill, Inc., New York, NY, 1993.
26. Farrow, K., and Kurama, Y., "Capacity-Demand Index Relationships for Performance-Based Seismic Design," Structural Engineering Research Report #NDSE-01-02, Department of Civil Engineering and Geological Sciences, University of Notre Dame, Notre Dame, IN, November 2001, (available for download at www.nd.edu/~concrete).
27. Farrow, K., and Kurama, Y., "Ground Motion Scaling Methods for Different Structure Characteristics and Site Conditions," *Earthquake Engineering and Structural Dynamics* (submitted for publication, March 2002).
28. Shome, N., and Cornell, C., "Normalization and Scaling Accelerograms for Nonlinear Structural Analysis," Sixth U.S. National Conference on Earthquake Engineering, Seattle, WA, May-June 1988 (CD-ROM).
29. Farrow, K., and Kurama, Y., "Capacity-Demand Index Relationships for Performance-Based Seismic Design," *Earthquake Spectra*, Earthquake Engineering Research Institute (submitted for publication, March 2002).

APPENDIX A — NOTATION

a_m = maximum absolute roof acceleration
$\overline{a}_m$ = average a_m under seven MIV-scaled ground motions
a_{me} = maximum absolute roof acceleration of emulative wall
a_{mp} = maximum absolute roof acceleration of unbonded post-tensioned wall
a_p = area of a post-tensioning bar
d_h = normalized inelastic energy dissipation
d_{hp} = normalized inelastic energy dissipation of unbonded post-tensioned wall
D = unfactored design dead load
D_h = inelastic energy dissipation per loading cycle
E_c = Young's modulus for concrete
E_p = Young's modulus for post-tensioning steel
E_{py} = post-yield stiffness of truss elements modeling post-tensioning bars
E_s = Young's modulus for mild reinforcing steel
f'_c = unconfined concrete compressive strength
f_{ct} = concrete tensile strength
f_{pi} = initial stress in post-tensioning bars
f_{pu} = ultimate strength of post-tensioning steel
f_{py} = yield strength of post-tensioning steel
f_{su} = ultimate strength of mild reinforcing steel
f_{sy} = yield strength of mild reinforcing steel
g = gravitational acceleration
G_d = axial force near base of wall due to unfactored design dead loads
G_l = axial force near base of wall due to unfactored unreduced design live loads
k_{sec} = secant stiffness of equivalent linear elastic system
l_w = wall length
L = unfactored unreduced design live load
MIV = maximum incremental velocity
n_c = number of roof drift peaks
$\overline{n}_c$ = average n_c under seven MIV-scaled ground motions
n_{cp} = number of roof drift peaks of unbonded post-tensioned wall
PGA = peak ground acceleration
PGV = peak ground velocity
r_{ae} = a_m/a_{me}
$\overline{r}_{ae}$ = average r_{ae} under seven MIV-scaled ground motions
r_{ap} = a_m/a_{mp}
$\overline{r}_{ap}$ = average r_{ap} under seven MIV-scaled ground motions
r_{cp} = n_c/n_{cp}
$\overline{r}_{cp}$ = average r_{cp} under seven MIV-scaled ground motions
$\overline{r}_{cp,60}$ = $\overline{r}_{cp}$ for $\delta_{cp} = 0.60$
$\overline{r}_{cp,70}$ = $\overline{r}_{cp}$ for $\delta_{cp} = 0.70$
$\overline{r}_{cp,80}$ = $\overline{r}_{cp}$ for $\delta_{cp} = 0.80$
$\overline{r}_{cp,90}$ = $\overline{r}_{cp}$ for $\delta_{cp} = 0.90$
r_{de} = Δ_m/Δ_{me}
$\overline{r}_{de}$ = average r_{de} under seven MIV-scaled ground motions
r_{dp} = Δ_m/Δ_{mp}
$\overline{r}_{dp}$ = average r_{dp} under seven MIV-scaled ground motions
r_{hp} = d_h/d_{hp}
$r_{hp,1}$ = d_h/d_{hp} for first roof drift cycle
$r_{hp,2}$ = d_h/d_{hp} for second roof drift cycle
$r_{hp,3}$ = d_h/d_{hp} for third roof drift cycle
$r_{hp,4}$ = d_h/d_{hp} for fourth roof drift cycle
r_{se} = ρ_s/ρ_{se}
R = response modification coefficient
t = time
t_w = wall thickness
T = fundamental (i.e., first) linear elastic period
U_e = energy absorbed by equivalent linear elastic system
V = base shear force
β = relative energy dissipation ratio
δ_c = Δ_c/Δ_m
δ_{cp} = Δ_c/Δ_{mp}
Δ = roof drift
Δ_c = maximum roof drift reached during a loading cycle/amplitude of roof drift peak
Δ_m = maximum roof drift during dynamic response
$\overline{\Delta}_m$ = average Δ_m under seven MIV-scaled ground motions
Δ_{me} = maximum roof drift during dynamic response of emulative wall
Δ_{mp} = maximum roof drift during dynamic response of unbonded post-tensioned wall
ε_{pu} = strain corresponding to f_{pu}
ε_{py} = yield strain of post-tensioning steel
ξ = viscous damping ratio
ρ_p = post-tensioning steel ratio
ρ_s = mild reinforcing steel ratio
ρ_{se} = mild reinforcing steel ratio of emulative wall
ρ_{sp} = spiral reinforcement ratio